Universiteit
Leiden
The Netherlands

Bioorthogonal labeling tools to study pathogenic intracellular bacteria

Bakkum, T.

Citation
Bakkum, T. (2021, November 17). *Bioorthogonal labeling tools to study pathogenic intracellular bacteria*. Retrieved from https://hdl.handle.net/1887/3240088

Version:	Publisher's Version
License:	Licence agreement concerning inclusion of doctoral thesis in the Institutional Repository of the University of Leiden
Downloaded from:	https://hdl.handle.net/1887/3240088

Note: To cite this publication please use the final published version (if applicable).

Chapter 5

Bioorthogonal Correlative Light-Electron Microscopy of *Mycobacterium tuberculosis* in Macrophages Reveals the Effect of Anti-Tuberculosis Drugs on Subcellular Bacterial Distribution

Published as:
Thomas Bakkum, Matthias T. Heemskerk, Erik Bos, Mirjam Groenewold, Nikolaos Oikonomeas-Koppasis, Kimberley V. Walburg, Suzanne van Veen, Martijn J.C. van der Lienden, Tyrza van Leeuwen, Marielle C. Haks, Tom H.M. Ottenhoff, Abraham J. Koster, Sander I. van Kasteren. *ACS Central Science*, **2020**; 6(11): 1997-2007

Abstract

Bioorthogonal Correlative Light-Electron Microscopy (B-CLEM) can give a detailed overview of multicomponent biological systems. It can provide information on the ultrastructural context of bioorthogonal handles and other fluorescent signals, as well as information about subcellular organization. In this chapter, B-CLEM is applied to the study of the intracellular pathogen *Mycobacterium tuberculosis* (*Mtb*) by generating a triply labeled *Mtb* through combined metabolic labeling of the cell wall and the proteome of a DsRed-expressing *Mtb* strain. Study of this pathogen in a B-CLEM setting was used to provide information about the intracellular distribution of the pathogen, as well as its in situ response to various clinical antibiotics, supported by flow cytometric analysis of the bacteria, after recovery from the host cell (*ex cellula*). The RNA polymerase-targeting drug rifampicin displayed the most prominent effect on subcellular distribution, suggesting the most direct effect on pathogenicity and/or viability, while the cell wall synthesis-targeting drugs isoniazid and ethambutol effectively rescued bacterial division-induced loss of metabolic labels. The three drugs combined did not give a more pronounced effect but rather an intermediate response, whereas gentamicin displayed a surprisingly strong additive effect on subcellular distribution.

5.1 Introduction

Mycobacterium tuberculosis (*Mtb*), the causative agent of tuberculosis (TB), is currently the deadliest pathogen in the world. It is responsible for approximately 10 million cases and 1.6 million deaths every year.[1] Moreover, a quarter of the world's population is estimated to be carrying the latent form of the disease.[1] All this has become even more urgent over the last few decades with multi-drug resistant (MDR-) and extensive drug resistant (XDR-) variants becoming increasingly prevalent.[1] Vaccine and drug development for *Mtb* has proven slow and challenging, in part due to the highly complex pathogen-host interactions, and lack of suitable antigens.[2,3]

The intracellular lifecycle of *Mtb* further affects this problem. Upon infection of host cell macrophages, its behavior is highly heterogeneous. Both fast, and slow growing forms of the bacteria exist[4,5]; the latter displaying tolerance to most of the available drugs.[6–12] This has resulted in the requirement for long treatment periods with cocktails of antibiotics, with the current standard of care being a six to nine-month course of rifampicin, isoniazid, ethambutol and/or pyrazinamide.[13] Treatment of MDR-TB requires more extensive antibiotic treatment, lasting up to 2 years, with poor side-effect profiles.[14] Recently, a new therapy for MDR-TB and XDR-TB was approved consisting of pretomanid in combination with bedaquiline and linezolid, and several others are currently under clinical development.[13]

Mtb is a facultative intracellular pathogen that primarily colonizes the lungs of patients by entering the upper and lower airways, through aerosol-transfer.[15] At these sites, *Mtb* is phagocytosed by alveolar macrophages, which – rather than clearing the pathogen – serve as their host cells.[16] The longstanding co-evolution of *Mtb* with humans has resulted in the emergence of many mechanisms by which *Mtb* can interfere with the cellular and organismal immune responses.[17] It can, for example inhibit phagosome acidification, block the recruitment of EEA1 and interfere with the Rab5-to-Rab7 conversion[18], resulting in the formation of a nutrient-rich compartment that favors survival and replication of the pathogen.[18,19] *Mtb* is also able to inhibit autophagy and apoptosis, effectively blocking all of the backup mechanisms for microbial killing.[20,21] Even if maturation of the phagosome does occur, *Mtb* is known to be strongly resistant to both acidic conditions (down to pH 4.5) and the reactive oxygen and nitrogen species (ROS/RNS) normally employed to kill phagosomal pathogens, by virtue of its thick cell wall[21], the production of antioxidative mycothiol (MSH)[21], and several neutralizing enzymes.[20,21]

It has recently been shown that the localization of *Mtb* within the cell is also a complex and highly dynamic process: some phagosomes are arrested in an early state, while the majority of phagosomes will follow the conventional maturation pathway, or a Rab20-dependent pathway to form a spacious phagosome.[22] Damaging of the phagosome allows the bacterium to avoid degradation or even escape to the cytosol, followed by rapid replication and host cell necrosis.[23] Recapture of the cytosolic bacteria may occur through ubiquitin-mediated autophagy, which again may lead to either autophagosome maturation or arrest.[24–26] The precise contribution of these stages to overall *Mtb* survival is not yet known, nor is the change in these processes during drug treatment, but it implicates a dynamic host-pathogen 'arms race'. Even if a successful immune response – usually supported by T-cell help – is mounted against *Mtb,* generally a subpopulation of so-called 'persister cells' remain in a dormant state. These bacteria have downregulated metabolic activity, upregulated stress-related genes, and as a result can establish a drug-tolerant, latent infection.[7]

This complex intracellular life cycle has made the study of *Mtb* difficult. Development of imaging techniques that allow the identification and study of the various stages of intracellular survival or killing of *Mtb* has long been sought after. Fluorescent protein-modified *Mtb* has allowed its imaging by confocal microscopy, but the reliability of fluorescent proteins varies and the fluorescence is lost upon degradation of the protein by the host.[27] Metabolic labeling of the mycobacterial cell wall, using fluorescent or bioorthogonal analogues of D-alanine[28,29] or trehalose[30–32], or using fluorescent antibiotic analogues has allowed the study of growing and dividing *Mtb*.[33–35] This has, for example, allowed the discrimination of live from dead *Mtb* in sputum samples.[32] Finally, a dual-targeting Activity-Based Probe (ABP) was recently reported, combining the activity of two *Mtb*-specific enzymes to obtain extremely high specificity for *Mtb* over other mycobacteria.[36] These approaches are, however, all based on fluorescent techniques. They – in view of the complex life cycle of *Mtb* in the host – therefore do not provide information on, for example, host compartments and other ultrastructural features during infection.

Electron microscopy (EM) provides ultrastructural information but has limited options for labeling specific components of the bacterium and host, compared to fluorescent labeling techniques. For the study of *Mtb*, EM has proven useful to delineate parts of its life cycle, such as phagosome maturation, perturbation and repair, as well as cytosolic entry and reuptake by autophagy.[22,25,37–39] Correlative techniques, in which light and electron microscopy are combined have proven to

be powerful by providing both structural and functional information in one multimodal dataset, that can be visualized in a single image. The combination of fluorescence microscopy and Transmission Electron Microscopy (TEM) is known as Correlative Light-Electron Microscopy (CLEM).[40] For the study of *Mtb,* CLEM has been used to show *Mtb* replication within necrotic macrophages[41], to discover a previously unknown niche for *Mtb* replication in the lymph nodes of TB patients[42], and to visualize the subcellular distribution of bedaquiline in *Mtb*-infected macrophages.[43]

In order to combine the information that metabolic labeling studies can provide on the intracellular life cycle of *Mtb* with the information on bacterial structure and host cell biology that CLEM can provide, these approaches were integrated (**Figure 1**). Previous studies have shown that an intracellular proteome labeled with alkyne or azide-containing amino acids can be selectively visualized by CLEM within a mammalian host cell (including degradation products stemming from the phagocytosed bacteria).[44,45] However, this only provided one parameter to study and in order to provide a useful imaging approach for intracellular *Mtb*, multiple parameters relating to the intracellular lifecycle of the bacterium had to be visualized in parallel.

To this end, two bioorthogonal labels are here used in parallel – one for labeling the proteome and one for labeling the peptidoglycan layer – as well as the expression of a fluorescent protein. These three parameters, in combination with ultrastructural information, can yield information on where the bacteria are localized intracellularly, whether the bacteria are dividing, and to what extent antibiotics exert their anti-microbial effects. The resulting pathogen, labeled with L-azidohomoalanine (Aha; incorporated into proteome), D-propargylglycine (alkDala; incorporated into peptidoglycan), and DsRed fluorescent protein (anabolic activity) is used to study its fate inside a macrophage cell line (**Figure 1**). Using a dual copper-catalyzed Huisgen cycloaddition (ccHc) 'click' reaction on thin sections, these three parameters could be studied in their ultrastructural context. The two handles could be consecutively reacted without apparent cross-reactivity between handles (no loss of signal or altered patterns were observed compared to single labels). This bioorthogonal-CLEM (B-CLEM) approach makes it possible to study the intracellular distribution of *Mtb* and link this information to the retention of the metabolic labels over time. Comparing these parameters between untreated cells and cells treated with rifampicin, isoniazid, ethambutol or a combination of the three, provided valuable insights into the subcellular effect of these clinical antibiotics. These observations were then further substantiated using a flow

cytometry-based assay that allowed a more thorough quantification of the label retention under these conditions. An overview of the chemical structures and mechanisms of action of the antibiotics used in this chapter can be found in **Figure S1**.

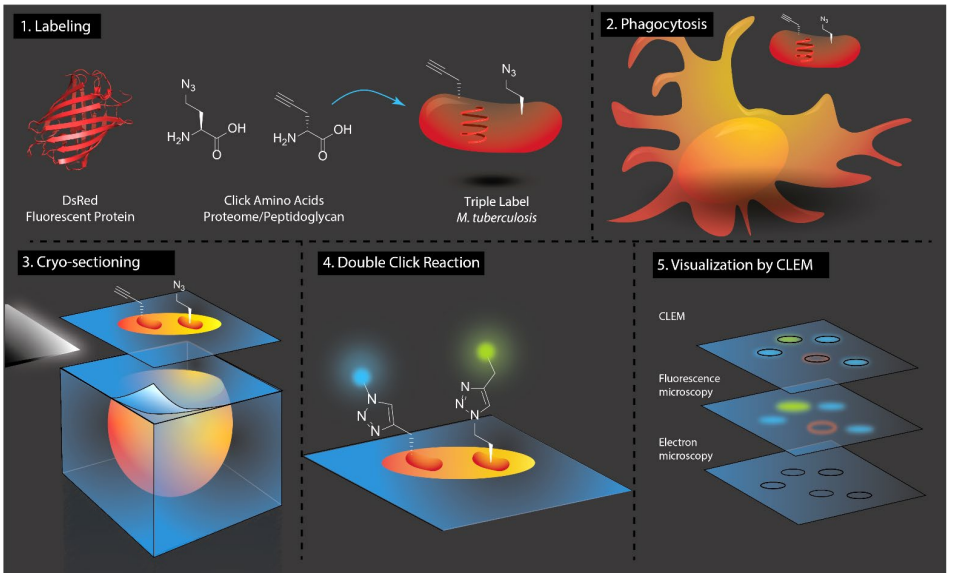

Figure 1. Bioorthogonal Correlative Light-Electron Microscopy (B-CLEM) strategy for *in situ* imaging of *Mtb*. Triple labeling of *Mtb* (**1**) is combined with two sequential on-section click reactions (**4**) and visualized with correlated fluorescence and electron microscopy (**5**) to provide information on the in-cell life cycle of *Mtb*.

5.2 Results and Discussion

5.2.1 Production and validation of triple-label *Mtb*.

The incorporation of bioorthogonal amino acids in *E. coli* and *S. enterica* serovar Typhimurium was previously optimized, based on the BONCAT-protocol developed by the Tirrell-lab.[46–49] Using in-gel fluorescence after ccHc of bacterial lysates, label incorporation into the bacterial proteome could be quantified on the population level. Flow cytometry of fixed bacteria allowed for the quantification of the label on a per-bacterium level.[44,45] These studies have yielded optimal labeling conditions consisting of a pulse with the bioorthogonal amino acid (4 mM) for approx. 1-2 doubling times (30 min in case of the above species), with increased incubation leading to reduced growth and viability.[44,45]

In order to optimize bioorthogonal amino acid-incorporation into the *Mtb*-proteome, the lysis conditions for *Mtb* were optimized first, to maximize protein recovery (and killing of the pathogen to allow handling outside the BSL-III facility). This was achieved with a combination of 1% SDS and heat treatment, as detergents alone were found to be insufficient for both killing and protein recovery (**Table 1**).

Table 1. Optimization of lysis conditions for analysis of label incorporation by in-gel fluorescence. The condition shown in bold was chosen as the optimal lysis method.

Lysis conditions	Fluorescence	Protein recovery
1% IGEPAL*[1]	+/--	- [2]
1% SDS[1]	+/-	- [2]
5% SDS[1]	+/-	- [2]
Lysozyme[3]; 1% IGEPAL*[1]	+	+/- [2]
Lysozyme[3]; 10% IGEPAL*[1]	-	- [2]
Lysozyme[3]; 1% IGEPAL* + 1% SDS[1]	+	++/-
Lysozyme[3]; heat[4]	-	-
Lysozyme[3]; 4% IGEPAL* + heat[4]	-	-
Lysozyme[3]; 4% SDS + heat[4]	+	+/-
Lysozyme[3]; 4% CHAPS + heat[4]	-	-
Lysozyme[3]; 6M urea + heat[4]	+/-	-
Lysozyme[3]; 1M NaCl + heat[4]	-	-
Lysozyme[3]; 4% CHAPS + 6M urea + 1M NaCl + heat[4]	+/-	-
Lysozyme[3]; 4% CHAPS + 4% IGEPAL* + 4% SDS + heat[4]	+/-	+/-
ddH_2O + heat[4]	+/-	-
1% SDS + heat[4]	**+**	**++**
1% SDS 30 min at 4°C; heat[4]	+/-	++
1% SDS 18 hours at -30°C; heat[4]	+/-	++
1% SDS added to growth culture + heat[4]	+/-	+++ [5]

* = IGEPAL CA-630; [1] = in 150 mM NaCl, 50 mM HEPES pH 8, O/N at 4°C; [2] = after 0.2 µm filtration to remove live/intact bacteria, due to insufficient killing of *Mtb* (!); [3] = 2 mg/mL lysozyme for 1 hour at 37°C; [4] = 30 min at 80°C, to guarantee sufficient killing of *Mtb* (!); [5] = may include potentially unwanted proteins from growth culture.

These lysis conditions were used to assess bioorthogonal amino acid incorporation by in-gel fluorescence, following SDS-PAGE. As the generation time of *Mtb* is approximately 24h, various conditions were explored, starting from 4 mM L-azidohomoalanine (Aha) or L-homopropargylglycine (Hpg) for 48h. Label incorporation plateaued around 48h, but labeling times >48h reduced cell growth; particularly for Hpg-treated cells (**Figure 2A**). Hpg was therefore excluded from further analysis.

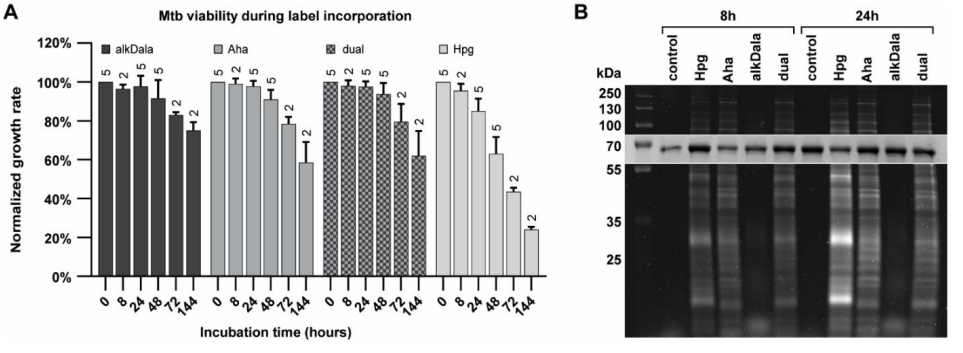

Figure 2. Production and validation of triple label *Mtb*. DsRed-expressing *Mtb* H37Rv were incubated with 4 mM Hpg, 4 mM Aha, 5 mM alkDala or a combination of 4 mM Aha and 5 mM alkDala (dual), for the indicated time in Middlebrook 7H9 broth. **A:** Bacterial viability during label incorporation was assessed by normalizing the growth rate (OD_{600} measurements) to control bacteria, grown in the absence of metabolic labels. The number of biological replicates for each OD_{600} measurement is indicated above the bar, error bars indicate standard deviation from the mean. **B:** Label incorporation throughout the proteome was analyzed by in-gel fluorescence, following bacterial lysis, ccHc reaction with AF647-azide (alkDala/Hpg) or AF647-alkyne (Aha/dual) and SDS-PAGE. Coomassie Brilliant Blue staining was used as a loading control; shown as an insert around the most prominent 60 kDa band, resulting from the DsRed-expression plasmid containing the Hsp60 promotor.[50]

Cell wall labeling conditions with D-propargylglycine (alkDala), a ccHc-reactive precursor in the cell wall synthesis, were inspired by Siegrist et al.[28] Single labeling experiments with Aha or alkDala showed that no detrimental effects on viability were observed up to 48h for either label in terms of viability (**Figure 2A**). Even extensively labeled *Mtb* (144h) seemed to recover their growth rate after medium exchange (**Figure S2**). It was next determined whether this was also the case for dual labeling with Aha and alkDala (**Figure 2A, Figure S2**). Co-incubation of *Mtb* with both labels did not enhance toxicity up to the 48h timepoint and revealed homogeneous proteome labeling (**Figure 2B**). The gel-based assay revealed that treatment of *Mtb* for 48h with both labels provided the highest label incorporation (combined with the most facile protocol).

To determine whether all cells incorporated the label to an equal extent, a flow cytometry-based assay was used. Again, previous protocols for bacterial fixation and permeabilization for flow cytometry were found to be incompatible with ccHc-reaction in *Mtb*. This was likely due to the thick (40-100 nm) and highly complex mycobacterial cell wall.[51] The mycobacterial cell wall contains multiple layers of (peptido)glycans and lipids, including the ultra-lipophilic mycolic acids that can be up to 90 carbons in length.[52] In practice, this results in hydrophobic aggregation of bacteria (especially after fixation) and an impermeability to the ccHc-reactive fluorophores. It is likely that this thick and impermeable cell wall reduces the yields of the two ccHc-reactions. A wide range of permeabilization conditions was explored, varying detergents, permeabilization and fixation conditions (**Table 2**). After this extensive optimization, it was found that the most effective conditions for permeabilizing the bacteria for flow cytometric analysis – that balanced the permeability with the structural integrity required to remain intact during ccHc reaction – are pre-treatment with 1% SDS for 15 minutes, followed by overnight fixation with 4% paraformaldehyde at room temperature (**Table 2**). Addition of BSA as an anti-clumping additive during staining steps (**Table 3**) was required to avoid hydrophobic aggregation of the fixed bacteria.

Table 2. Optimization of fixation & permeabilization conditions for analysis of label incorporation by flow cytometry. The condition shown in bold was chosen as the optimal fixation/permeabilization method.

Fixation conditions	Permeabilization conditions	Aha-click positive
2% PFA[1]	Lysozyme[2]; 0.1% IGEPAL*[3]	7%[4]
2% PFA[1]	Lysozyme[2]; 1% SDS[3]	18%[4]
2% PFA[1]	Lysozyme[2]; 0.1% IGEPAL* + 1% SDS[3]	12%[4]
2% PFA[1]	Lysozyme[2]; 1% IGEPAL* + 1% SDS[3]	9%[4]
2% PFA[1]	Lysozyme[2]; 1% SDS[3]	14%[4]
2% PFA[1]	Lysozyme[2]; 2% SDS[3]	22%[4]
2% PFA[1]	Lysozyme[2]; 4% SDS[3]	21%[4]
2% PFA[1]	Lysozyme[2]; 1% SDS + 5 mM EDTA[3]	19%[4]
2% PFA[1]	Lysozyme[2]; 2% SDS + 5 mM EDTA[3]	26%[4]
2% PFA[1]	Lysozyme[2]; 1% SDS + 1% EtOH[3]	16%[4]
2% PFA[1]	Lysozyme[2]; 2% SDS + 1% EtOH[3]	18%[4]
2% PFA/0.1% SDS[1]	Lysozyme[2]; 2% SDS + 5 mM EDTA[3]	18%[4]
2% PFA/0.1% SDS[1]	Lysozyme[2]; 2% SDS + 10 mM EDTA[3]	20%[4]
2% PFA/0.1% SDS[1]	Lysozyme[2]; 2% SDS + 100 mM EDTA[3]	29%[4]
2% PFA/0.1% SDS[1]	Lysozyme[2]; 2% SDS + 200 mM EDTA[3]	29%[4]
4% PFA[1]	None	17%[4]
8% PFA[1]	None	33%[4]
4% PFA/0.1% SDS[1]	None	53%[4]
1% SDS; 4% PFA/0.1% SDS[1]	None	70%[4]
1% SDS; 4% PFA/0.1% SDS[1]	0.1% SDS[5]	61%[5]
1% SDS; 4% PFA/0.1% SDS[1]	Lysozyme[2]; 2% SDS + 10 mM EDTA[3]	57%[5]
1% SDS; 4% PFA/0.1% SDS[1]	0.1% Tween[#6]	22%[6]
1% SDS; 4% PFA/0.1% SDS[1]	Lysozyme[2]; 0.1% Triton[‡] + 0.1% Tween[#3]	19%[6]
1% SDS; 4% PFA[1]	None	63%[7]
1% SDS; 4% PFA[1] at RT	**None**	**76%[7,8]**
4% PFA[1] at RT	None	4%[7]
4% PFA[1] at RT	Lysozyme[2] for 30 min at 37°C	39%[7]
4% PFA[1] at RT	Lysozyme[2] for 60 min at 37°C	51%[7]
4% PFA[1] at RT	Lysozyme[2] for 90 min at 37°C	59%[7]
4% PFA[1] at RT	Lysozyme[2] for 90 min at 37°C; 0.1% Triton[‡]	70%[7]
4% PFA[1] at RT	Lysozyme[2] for 90 min at 37°C; 0.5% Triton[‡]	69%[7]
4% PFA[1] at RT	Lysozyme[2] for 90 min at 37°C; 0.1% SDS	64%[7]

* = IGEPAL CA-630; # = Tween-80; ‡ = Triton-X100; [1] = in PBS for ≥18h at 4°C, unless otherwise specified; [2] = 2 mg/mL lysozyme for 60 min at 37°C, unless otherwise specified; [3] = in PBS; [4] = no anti-clumping agent used, resulting in a very low yield after staining; [5] = 0.1% SDS used as anti-clumping agent during all washing steps; [6] = 0.1% Tween-80 used as anti-clumping agent during all washing steps; [7] = 0.1% BSA used as anti-clumping agent during all washing steps; [8] = higher signal observed for alkDala, compared to other conditions

Table 3. Anti-clumping additives to reduce hydrophobic aggregation of fixed *Mtb* during washing steps, during sample preparation for flow cytometry. The condition shown in bold was considered optimal.

Anti-clumping additive	Effect on aggregation	Effect on yield
0.1% Tween[#] in PBS	++	+/- [1]
0.1% SDS in PBS	+	- [2]
0.1% gelatin[†] in PBS	+	+/-
0.1% BSA in PBS	**+**	**+**

[#] = Tween-80; [†] = gelatin from cold water fish skin; [1] = loss of alkDala signal due to apparent over-permeabilization (dismissed); [2] = loss of Aha due to apparent over-permeabilization.

Despite this extensive set of optimization experiments, a subpopulation of DsRed positive events (~25%) remained unlabeled by both click reactions, perhaps due to them being permeabilization resistant, metabolically inactive or even dead prior to labeling.[7,53] These unlabeled bacteria were excluded from quantification by gating for the double positive (Aha+/alkDala+) quadrant (**Figure 3A**, **Figure S3**). To confirm that the observed label incorporation was indeed selective and related to metabolic activity, it was shown that pre-incubation with Rifampicin for 1h and 24h respectively reduced or abolished Aha-incorporation at 0.1, 1.0 and 10 µg/mL (**Figure S4**). The cell wall inhibitor D-cycloserine achieved the same for alkDala incorporation (**Figure S5**). Heat killing (**Figure S6B**) or paraformaldehyde fixation (**Figure S6C**) abolished the incorporation of both labels. With these restrictions applied, label incorporation for Aha and alkDala seemed to follow a similar trend as observed for the SDS-PAGE assay. Incorporation of both labels plateaued at 48 hours incubation, in high signal-to-background ratios (**Figure 3A-viii**).

5.2.2 Bioorthogonal CLEM as a multi-parameter analysis method to study intracellular *Mtb*.

After successfully constructing triple label *Mtb*, their compatibility with B-CLEM was assessed (**Figure 3B**, Figure 4). To this end, DsRed-expressing *Mtb* were incubated with Aha (4 mM) and alkDala (5 mM) simultaneously for 48 hours for maximum label incorporation. The bacteria were prepared for cryo-sectioning, according to the Tokuyasu method.[54–56] Briefly, samples were fixed with paraformaldehyde and glutaraldehyde (2% w/v and 0.2% w/v respectively for 2 hours), after which the bacterial pellet was rinsed with PBS and embedded in 12% gelatin. Millimeter-sized cubes were prepared manually, followed by sucrose infiltration and plunge-freezing on sample pins. Ultrathin cryo-sections (75 nm) were prepared and transferred to a Formvar/carbon-coated titanium TEM-grid. Thawed cryo-sections were subjected to on section click-reaction with AF647-azide or AF647-alkyne for equal comparison between Aha and alkDala incorporation. Using these

experiments, the label incorporations could be confirmed (with the sectioning being used in lieu of permeabilization). Both alkDala and Aha were minimally detectable after 1 hour with the signal increasing upon longer incubation (**Figure 3B**). Optimal label incorporation is observed after 48 hours without any noticeable effect on DsRed fluorescence. No detectable background fluorescence was observed for the unlabeled control samples (**Figure S7**).

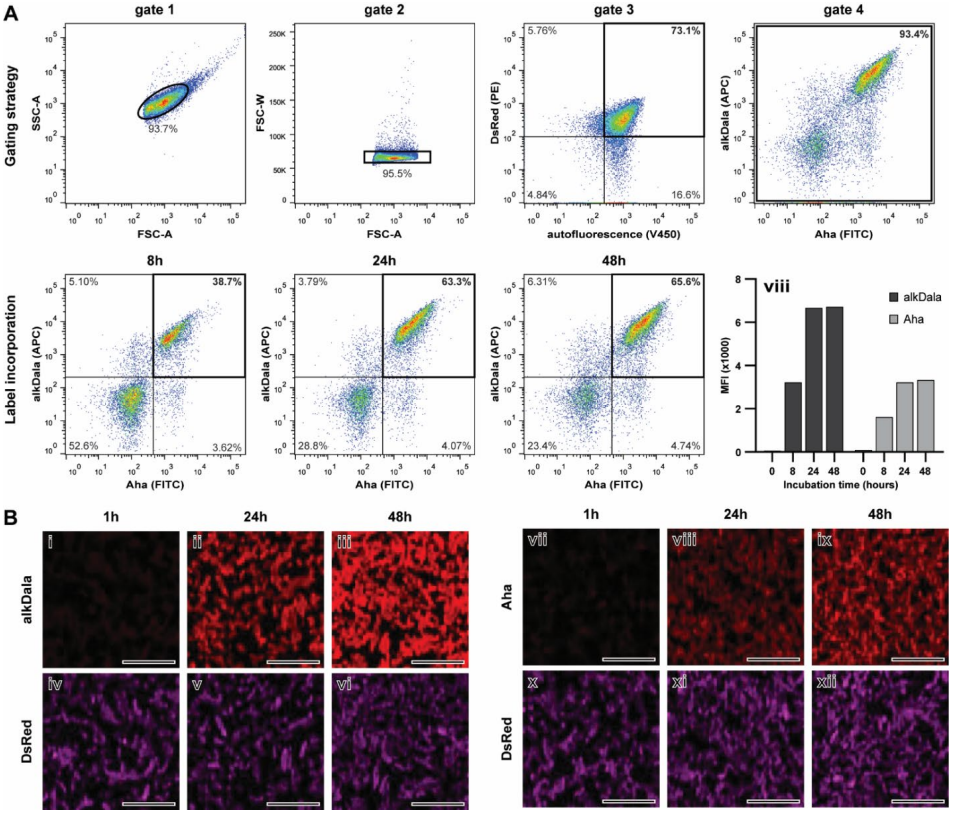

Figure 3. Optimization of label incorporation. DsRed-expressing *Mtb* H37Rv were incubated with 4 mM Aha, 5 mM alkDala or a combination of 4 mM Aha and 5 mM alkDala (dual), for the indicated time in Middlebrook 7H9 broth. **A**: Label incorporation per bacterium was quantified by flow cytometry after sequential ccHc reaction with AF647-azide (alkDala) and AF488-alkyne (Aha) on fixed and permeabilized bacteria. Bacteria were selected based on size (gate 1), shape (gate 2), fluorescence (gate 3) and exclusion of extreme outliers (gate 4). Quantification of the label incorporation was achieved by selecting the median fluorescence intensity (MFI) of the major [Aha+/alkDala+] population for dually-labeled *Mtb* or the major [Aha-/alkDala-] population for unlabeled *Mtb*. Controls and normalized MFI values are shown in Figure S2. **B**: Triple label *Mtb* were processed for cryo-sectioning, followed by ccHc reaction with AF647-azide (alkDala) or AF647-alkyne (Aha), to confirm the increase in label incorporation over time on ultrathin sections that can be directly used for CLEM. All scale bars represent 5 µm.

Next, these single bacteria were subjected to B-CLEM as follows. Fresh sections were prepared and subjected to double on-section click-reaction with AF647-azide and AF488-alkyne, with washing in between. The labeled sections were first imaged by confocal microscopy, then stained with uranyl acetate and finally imaged by TEM. The resulting images were then correlated using Photoshop to obtain the final CLEM images (**Figure 4**, **Figure S8**). These CLEM images show that >80% (n=200) of bacteria were positive for alkDala, Aha and/or DsRed, suggesting sub-optimal permeabilization was responsible for the incomplete labeling observed by flow cytometry above. The proteome label Aha colocalized largely with the fluorescent protein DsRed.

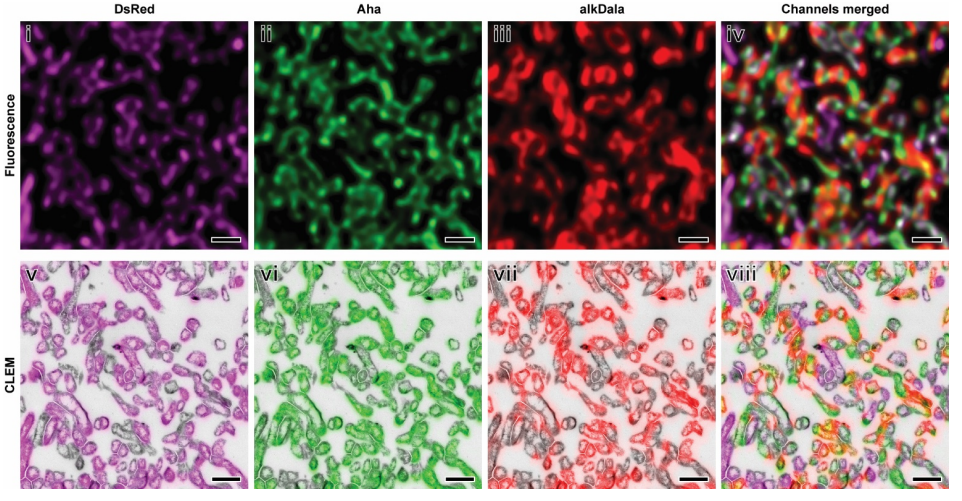

Figure 4. Bioorthogonal CLEM of triple label *Mtb* in vitro. Triple label *Mtb* were processed for cryo-sectioning, followed by sequential ccHc reaction with AF647-azide and AF488-alkyne. The fluorescently-labeled sections were imaged by confocal microscopy, followed by TEM and the images were correlated to obtain the CLEM image. The lower panel shows details from the large field of view CLEM image presented in Figure S4. The top panel shows the corresponding fluorescence channels separately for clarity. All scale bars represent 1 µm.

To explore the possibility of studying intracellular *Mtb* localization and processing, a murine (LPS-stimulated) macrophage cell line (RAW 264.7)[57,58] was infected with the double labeled DsRed-positive *Mtb* (MOI 25). The goal was to study whether signs of viability could be extrapolated from the information-dense CLEM images, containing both the ultrastructural information of EM and the functional information of the multi-label fluorescence microscopy. After Tokuyasu sample preparation, large field of view CLEM images containing over 100 cell-profiles per image could be obtained at 11,000x magnification by applying an in-house developed EM-stitching algorithm.[59] This approach provides a large dataset for qualitative and quantitative analysis of EM structures, guided by the fluorescence (illustrated in **Figure S9**). As observed in previous EM studies[19,60], the mycobacterial cell wall shows a typical electron translucent layer, representing the mycomembrane (MM), enclosed by an electron-dense outer layer (OL) and the peptidoglycan layer (PGL) (**Figure 5i**). The bacterial cell wall is delineated by the signal distribution of alkDala (**Figure 5iv**). *Mtb* was found to be spread over different compartments, such as small or tight vacuoles (**Figure 5v**, **Figure S10B**), large or spacious vacuoles (**Figure 5ix**, **Figure S10C**), or what appeared to be non-membrane-bound compartments (which could be due an insufficient membrane preservation on EM) (**Figure 5i**, **Figure S10A**). The presence of *Mtb* in these apparently non-membrane-bound compartments suggests escape from the parasitic vacuole to the cytosol, as reported in multiple studies.[19,23,61–64] In some cases, a double membrane was observed in proximity of an apparently cytosolic bacterium (**Figure S9D**, **Figure S10A-iv**), which is a hallmark of autophagy[65], implying that this process may occur.

At 24 hours post-infection, 23% of bacteria were found in small vacuoles, 72% in large vacuoles and 5% with no detectable membrane (n>500 bacteria counted). Additionally, a small percentage of bacteria (<5% of total) was found extracellularly, surrounded by cell debris (illustrated in **Figure S11A/B**). Many large vacuoles contained both bacteria and cell debris, suggesting the bacteria could have escaped from the previous host cell[23,66], before reuptake by another macrophage (**Figure S11B**). If host cell necrosis occurs, the plasma membrane integrity is lost, causing the cell to fall apart, which allows the bacteria to escape. However, if the host cell initiates apoptosis, the entire cell including bacteria can be taken up by a neighboring macrophage in a process called efferocytosis.[67] Distributions of bacteria indicative for either secondary phagocytosis of *Mtb*, following necrosis of the host cell (**Figure S11C-i**) or efferocytosis, when the entire apoptotic cell is internalized (**Figure S11C-ii**), were observed.

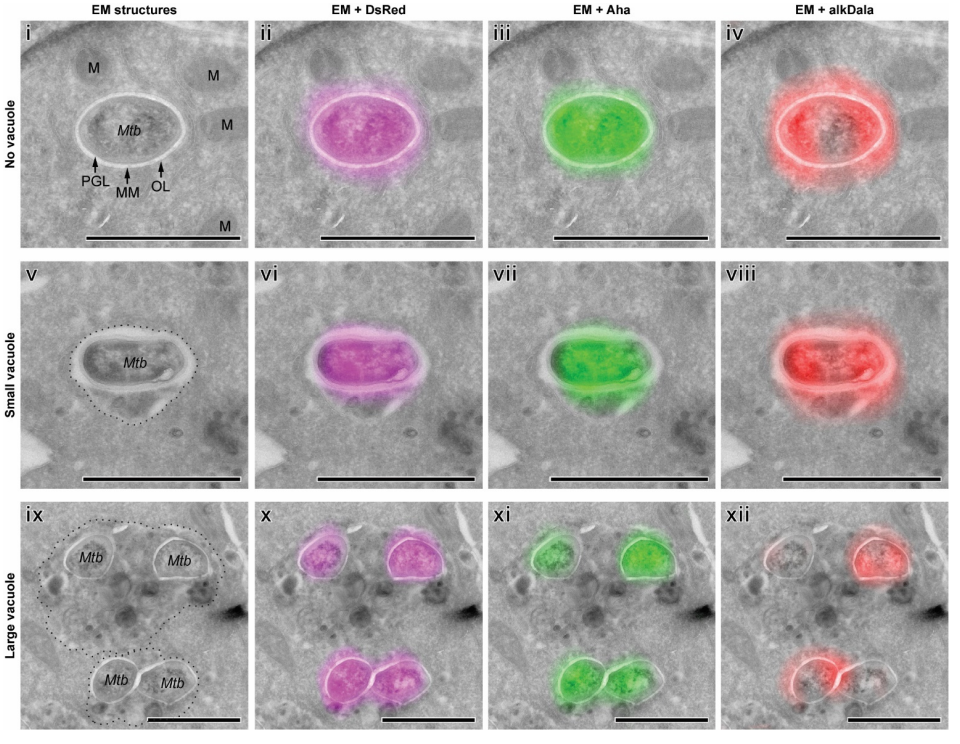

Figure 5. Bioorthogonal CLEM of triple label *Mtb* in RAW 264.7 macrophages. Triple label *Mtb* were processed for cryo-sectioning, followed by sequential ccHc reaction with AF647-azide and AF488-alkyne, and counterstaining with DAPI. Fluorescently-labeled sections were imaged by confocal microscopy, followed by TEM and the images were correlated to obtain the CLEM image. The fuzziness of the fluorescent signal is a result of the difference in resolution between the techniques as governed by the Abbe-limit of diffraction. Representative examples of intracellular triple label *Mtb* are shown, not within a vacuole (**i-iv**), in a small/tight vacuole (**v-viii**), or in a large/spacious vacuole (**ix-xii**). Small field of view CLEM images with separated fluorescence channels are shown for clarity. Corresponding large field of view image is presented in Figure S5. N = nucleus, M = mitochondria, PGL = peptidoglycan layer, MM = mycomembrane, OL = outer layer. A dotted line indicates the apparent vacuole where relevant. All scale bars represent 1 µm.

5.2.3 Bioorthogonal CLEM of *Mtb*-infected macrophages reveals the effect of antibiotics on the bacterial integrity and intracellular processing.

To determine how the intracellular distribution and fluorescent signals of triple label *Mtb* would be affected by the commonly-used antibiotics used in the treatment of tuberculosis, the experiment was repeated in the presence of rifampicin, isoniazid, ethambutol or a combination of the three for 24 hours. All drugs except ethambutol alone induced a significant alteration in the intracellular distribution of the bacteria (**Figure 6A**), with the triple-antibiotic cocktail showing the most pronounced effect, with 15% of bacteria residing in small vacuoles, 84%

in large vacuoles and only 1% did not appear to be within a vacuole (n>500). Interestingly, when cells were incubated with heat-killed bacteria, 95% of all bacteria were found in large vacuoles, with <0.5% present in structures without a detectable membrane. The individual drugs had less pronounced effects on distribution (**Figure 6A**). Rifampicin caused the largest shift in sub-cellular localization, with 12% of bacteria residing in small vacuoles, 85% in large vacuoles and 3% not within a vacuole (n>500). Isoniazid had a less pronounced effect, with 20% of bacteria in small vacuoles, 78% in large vacuoles and 3% not within a vacuole (n>500). Ethambutol did not show a significant difference compared to the control.

A large percentage of bacteria were found to be extracellular upon treatment with isoniazid (41% of total, n>500) or ethambutol (12% of total, n>500; Figure S12A), suggesting different drug mechanisms of action are involved. In addition, isoniazid treatment appeared to increase the occurrence of apparent host cell death (37%, n>500), while ethambutol appeared to decrease host cell death (2%, n>500; Figure S12B). These findings imply a need to reconsider the standard infection protocol, in which the infected cells are co-incubated with a low concentration of gentamicin (5 µg/mL) to kill off extracellular bacteria. During the 24 hours of incubation, many bacteria may escape from the host cell, which would then be exposed to the extracellular gentamicin before being taken up by another macrophage. This could result in an artificially high number of dead bacteria, thereby skewing the relative intracellular sub-populations. To confirm this hypothesis, *Mtb*-infected cells were incubated with or without the triple-antibiotic cocktail, in the presence or absence of gentamicin, for 24 hours and processed for CLEM. Indeed, a significant effect on the intracellular distribution was observed for both the triple-antibiotic cocktail and the untreated cells, when comparing the presence or absence of gentamicin (Figure 6B). Interestingly, a similar effect can be observed when comparing the triple-antibiotic cocktail to the control, either with gentamicin or without. This implies an additive drug effect for gentamicin, on top of the other antibiotics. Indeed, *Mtb*-infected cells in the complete absence of antibiotics showed only 50% of the bacteria residing in large vacuoles versus 31% in small vacuoles and 19% without an apparent vacuole (n>500). Gentamicin was therefore excluded from all further experiments.

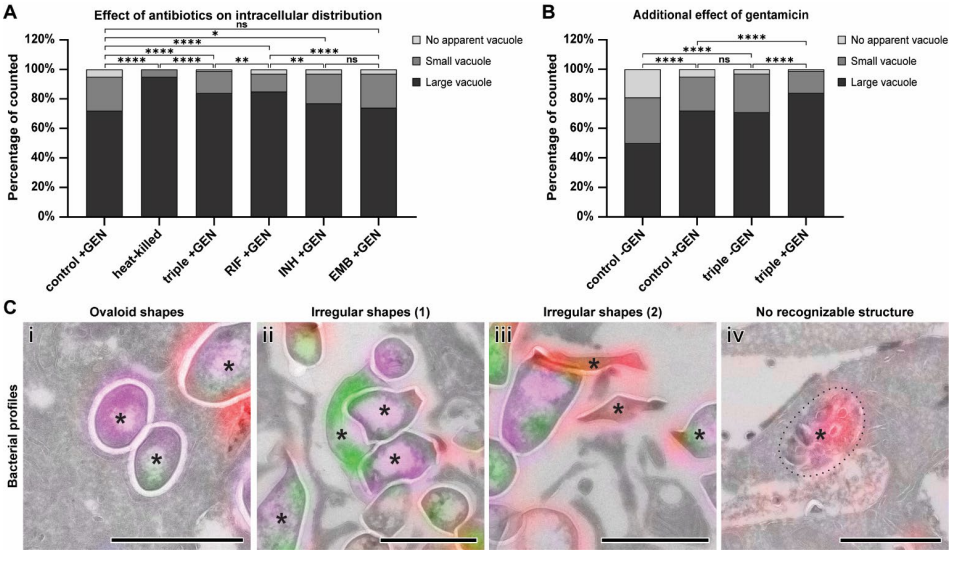

Figure 6. The effect of different antibiotics on the intracellular distribution and shape of triple label *Mtb* in RAW 264.7 macrophages. **A:** Intracellular distribution of *Mtb* was manually classified as not within a vacuole (none), small/tight vacuole (small) or large/spacious vacuole (large), after 24 hours of incubation with rifampicin (RIF), isoniazid (INH), ethambutol (EMB), triple antibiotics cocktail (triple), or without antibiotics (control). Shown as percentage relative to total number of intracellular *Mtb* counted in the analyzed region; n>500 for all. **B:** The additional effect of gentamicin (GEN) on the intracellular distribution of *Mtb* was assessed after 24 hours of incubation with triple antibiotic cocktail (triple +/-GEN) or without antibiotics (control +/-GEN). Raw distributions were pairwise compared using the chi-square test and corrected for multiple testing using the Benjamini-Hochberg procedure, with a false discovery rate (FDR) of 0.1 (****: p<0.0001, **: p<0.01, *: p<0.05, ns: not significant). **C:** Zoom-in CLEM examples of the most common shapes, observed for bacterial profiles, classified as ovaloid (i), irregular (ii/iii) or no recognizable structure (iv; enhanced contrast of fluorescence for visual purposes). Relevant structures are indicated with an asterisk (*). A dotted line indicates the apparent vacuole where relevant. All scale bars represent 1 µm.

In addition to the intracellular distribution of *Mtb*, the shape of the bacterial profile appeared to be affected by the antibiotics as well. After (cryo-)sectioning of the rod-shaped *Mtb*, the expected bacterial profile is somewhere between circular and elongated, but always ovaloid in shape (**Figure 6C-i**). Indeed, the bacterial profiles after 24h intracellular incubation without antibiotics were primarily ovaloid in shape (69%, n>500; **Figure S14D**). The remaining bacterial profiles display an irregular 'pointy' shape (**Figure 6C-ii/iii**, **Figure S14B**), perhaps suggesting a loss of bacterial integrity prior to fixation. Triple antibiotics treatment appeared to increase the number of irregular profiles (57%, n>500; **Figure S14D**), which may indicate an increase in *Mtb* killing. Some vacuoles were even found to contain distinct fluorescence while entirely lacking any recognizable bacterial structure

(**Figure 6C-iv**, **Figure S14C**), potentially carrying degradation products of the labeled *Mtb*. Interestingly, heat-killed bacteria were predominantly observed as irregular shapes (95%, n>500; **Figure S14D**) but with a well-preserved cell wall.

The early intracellular population of *Mtb*, immediately after infection, was highly concentrated in large vacuoles (>80%, n>200). At this time point (0h post-infection), no significant effect of antibiotic pre-treatment (24 hours triple-antibiotic cocktail in vitro, before infection) on the subcellular distribution (**Figure S13A**) nor on the bacterial profiles of *Mtb* (**Figure S14F**) was observed, suggesting that more time is required for processing of the bacteria by the host cell. The untreated bacteria do appear to reside more in large clusters of smaller vacuoles, while the pre-treated bacteria were mostly found in large and spacious vacuoles (See **Figure S13B** for examples). However, this classification criterion was too subtle for unbiased manual quantification and was therefore excluded from further analysis.

5.2.4 CLEM and flow cytometry-based quantification of label retention upon antibiotic treatment.

The average fluorescence intensity, resulting from the metabolic labels Aha and alkDala, can be used as a measure for bacterial division, as the label content per bacterium will 'dilute' upon division. By combining existing Photoshop tools with a custom-build JavaScript, as well as a custom-build ImageJ macro, it was possible to quantify the average fluorescence intensity per bacterium-profile from the CLEM images (i.e. multimodal datasets). Using this method, the bacteria were segmented out of the finely correlated CLEM image, and the mean fluorescence intensity (MFI) was analyzed for each of the three fluorescence channels (n>200 bacteria analyzed). These results show that intracellular *Mtb*, treated with the triple-antibiotic cocktail, retain more Aha and lose DsRed compared to the untreated control (**Figure 7A**, **Figure S15**). No significant difference in alkDala retention was observed (**Figure 7B**), although analysis artifacts cannot be excluded, due to the smudging of alkDala fluorescence beyond the selected bacterial outline (**Figure S15**) or variations in section thickness that may affect the fluorescence intensity.

Since quantification of CLEM is intrinsically limited by its laborious correlation procedure, a higher-throughput technique was required for unambiguous quantification of the effect of antibiotics on bacterial proliferation, to support the observations done in CLEM. To achieve this, a custom flow cytometry-based method was developed to analyze the bacteria after recovery from the infected host cells (*ex cellula*). This was achieved by selective host cell lysis (adapted from Liu et al.[68]), followed by fixation and click labeling of the recovered bacteria, using

the method described above, to obtain optimal signal-to-noise and optimal recovery of bacteria. The cytometry results show a clear loss of Aha and alkDala retention per bacterium over time (24h vs 0h control), in the absence of antibiotics (**Figure 7B**, **Figure S16**). This loss was largely avoided by isoniazid and ethambutol. Heat-killed bacteria showed no loss of label over time (**Figure S17J**). Rifampicin does not show an effect on label retention, suggesting a different mechanism of action (**Figure 7B**, **Figure S16**, **Figure S17**). The triple-antibiotic cocktail showed an intermediate effect on label retention, suggesting a combinatorial but non-additive effect on label retention. No significant effect on DsRed was observed for any of the antibiotics, through this quantification approach. However, isoniazid and ethambutol show a distinct reduction in the typical *Mtb* autofluorescence[69], similar but to a smaller degree as heat-killed *Mtb* (**Figure S17F**). This reduction in autofluorescence has previously been suggested as an indication for mycobacterial viability.[70]

Taken together, these results indicate that – within the context of an LPS-stimulated murine macrophage infection system – rifampicin mostly affects *Mtb* pathogenicity, while isoniazid and ethambutol seem to affect *Mtb* division more directly; although the complexity and heterogeneity of the life cycle of *Mtb* in host cells remains profound.

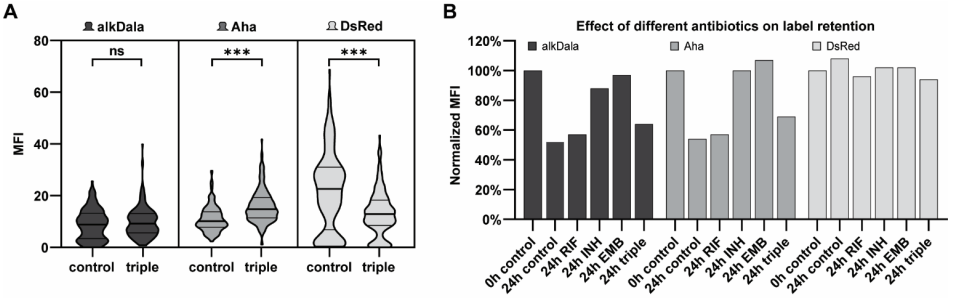

Figure 7. Quantification of label retention after intracellular incubation of triple label *Mtb* in RAW 264.7 macrophages with antibiotics. **A**: CLEM-based semi-automatic quantification of label retention after 24 hours intracellular incubation with triple antibiotics cocktail (triple) or without antibiotics (control). Distribution of the mean fluorescence intensity per bacterial profile (n=200). Thick horizontal line represents population mean, thin horizontal lines represent standard deviation (***: $p<0.001$, ns: not significant, Mann-Whitney U test). **B**: Flow cytometry-based quantification of label retention ex cellula, after 24 hours intracellular incubation with rifampicin (RIF), isoniazid (INH), ethambutol (EMB), triple antibiotic treatment (triple) or without antibiotics (24h control), normalized on bacteria recovered immediately after infection (0h control). Corresponding dot plots and MFI values, before normalization, are shown in Figure S12.

5.3 Conclusion

The here-described combinatorial method allows for the study of intracellular localization of pathogenic bacteria *in situ*, as well as the effect of clinical or experimental drugs on the entire host-pathogen system. By combining fluorescent protein expression, proteome and cell wall labeling with high-content CLEM and flow cytometry, new information about the complex intracellular behavior of *Mtb* in macrophages was obtained. CLEM allows for simple fluorescence-guided detection of bacterial structures, and inversely, EM-guided analysis of fluorescent labels. The ultrastructural information of EM provides a subcellular description of both the bacterial behavior and that of the host cell. In addition, flow cytometry provides a quantification method for bacterial label retention under varying conditions. Using a triple labeling strategy, different components of the bacterium could be visualized, providing multi-parameter information about the metabolic state of the pathogen, although the sought-after *in vivo* unambiguous identification of live, dormant and dead bacteria remains elusive. Using multiple labels also significantly reduces the chance of missing events due to absence of a fluorescent label, and at the minimum, provides an internal standard for equivalent labels (Aha and alkDala). Alternatively, using a single bioorthogonal label could bypass the arduous task of genetically labeling a complicated level-3 pathogen, like *Mtb*.

Large differences were observed between intracellular distribution of *Mtb* under normal conditions versus treatment with various clinical antibiotics. Rifampicin displayed the clearest effect on distribution, while isoniazid and ethambutol only had a mild effect. These observations suggest a more direct effect of rifampicin on bacterial pathogenicity and/or viability, which is in agreement with its proposed mechanism of action.[71] Surprisingly, a routine low dose of gentamicin displayed a strong effect on distribution, which was additive to both untreated cells or cells treated with all three antibiotics simultaneously. This effect of gentamicin was probably due to bacteria escaping from the host cell, undergoing gentamicin-induced extracellular killing, followed by re-internalization by surrounding macrophages. Although the additive effect of gentamicin is unlikely to interfere with routine assays, it should still be considered as a potential bias on drug efficacy.

Besides broadly occurring phenomena, such as the subcellular distribution of *Mtb*, many less common events were observed such as apparent phagosome-lysosome fusion, possible autophagy of cytosolic *Mtb*, partially degraded *Mtb* fragments, leakage and vesicular transport of fluorescently labeled *Mtb* components, bacterial lipid inclusions and exocytosis of mycolic acids. Although these observations could

not yet be supported by sufficient evidence, they present an interesting starting point for follow-up studies, highlighting the exploratory power of CLEM.

Flow cytometry-based quantification of label retention showed a clear loss of label retention over time, that was almost completely rescued by isoniazid or ethambutol treatment, but to a far lesser extent by rifampicin or the triple antibiotics combination. Label dilution over time is expected due to bacterial division without additional metabolic labels present in the medium. Label retention over time is therefore a result of inhibition of bacterial division, which is in accordance with the proposed mechanism of action for these antibiotics.[71] Perhaps most surprising is the apparently intermediate efficacy of the triple antibiotic combination in terms of label retention. However, since the triple antibiotic combination showed the most pronounced effect on intracellular distribution, the overall therapeutic effect is likely a combination of bacteriostatic and bactericidal effects, as can be expected from these antibiotics. If future research provides a way to unequivocally distinguish dead from live *Mtb*, this would greatly benefit the interpretation of these results and assist in the discovery of novel antibiotics.

5.4 Experimental

Safety statement

All biological experiments with *M. tuberculosis* described in this study were performed under strict Bio Safety Level 3 conditions. Following fixation and disinfection of the tubes, further sample preparation for CLEM was performed under normal laboratory conditions. No unexpected or unusually high safety hazards were encountered.

Reagents

Difco Middlebrook 7H9 broth and ADC growth supplement were purchased from Becton Dickinson, Breda, The Netherlands. Hygromycin B, gentamicin and azide- or alkyne-modified Alexa Fluor dyes (AF488 and AF647) were purchased from Thermo Fisher Scientific, Bleiswijk, The Netherlands. Dulbecco's modified Eagle medium (DMEM), GlutaMAX, Copper(II) sulfate pentahydrate, (+)-sodium L-ascorbate, tris(3-hydroxypropyltriazolylmethyl)amine (THPTA), aminoguanidine hydrochloride, paraformaldehyde, glycine, gelatin type A bloom 300 (gelatin), cold water fish skin gelatin, Lysozyme from hen egg white, bovine serum albumin (BSA), IGEPAL CA-630, Triton-X100 and Tween-80 were purchased from Sigma-Aldrich, Zwijndrecht, The Netherlands. D-propargylglycine (alkDala) was purchased from Combi-Blocks, San Diego, USA. EM-grade 8% paraformaldehyde and EM-grade 8% glutaraldehyde were purchased from Aurion, Wageningen, The Netherlands. Fetal calf serum (FCS) was purchased from VWR International, Amsterdam, The Netherlands. Penicillin G sodium and streptomycin sulphate were purchased from Duchefa, Haarlem, The Netherlands.

Organic synthesis

Synthesis of (S)-2-amino-4-azidobutanoic acid (L-azidohomoalanine; Aha)

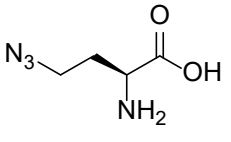

Aha was synthesized according to a previously described procedure by Zhang et al., 2010[72].

^{1}H-NMR (D_2O), 400 MHz: δ [ppm] = 4.05 (t, 1H, α-CH), 3.55 (t, 2H, γ-CH_2), 2.15 (m, 2H, β-CH_2).

Synthesis of (S)-2-Aminohex-5-ynoic acid (L-homopropargylglycine; Hpg)

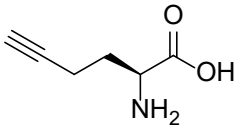

Hpg was synthesized according to previously described procedure by Li et al.[73], adjusted to obtain the enantiomerically pure L-Hpg variant based on Chenault et al.[74], Biagini et al.[75] and Dong et al.[76]

Chiral deprotection of *N*-acetyl-DL-homopropargylglycine (2-acetamidohex-5-ynoic acid)

A solution of 303 mg (1.13 mmol, 1 eq.) *N*-acetyl-DL-homopropargylglycine in 20 mL H_2O and adjusted to pH 7.5 using 1M NH_4OH. 1 mg kidney acylase I (≥2000 units/mg) was added and the mixture was stirred for 16 h at 37 °C. The enzyme was recovered by centrifugation dialysis, using a 10kDa membrane at 4000 rpm for 35 min at 10 °C. Next, the solution was acidified to pH 3 with 2M HCl and extracted with 3 x 20 mL diethyl ether. The organic layers were concentrated to retrieve the *N*-acetyl-D-homopropargylglycine. The aqueous layer was loaded on a pre-washed and regenerated Dowex 50WX8 cation exchange resin (60 mL). The column was washed with 5 x bed volume of water, maintaining a pH of 5.5 at the exit and eluted with 200 mL 1.5M NH_4OH. Product was detected by TLC and the eluate was concentrated and lyophilized to yield chirally pure L-Hpg (68 mg, 0.535 mmol, 95%) as a white powder.

^{1}H NMR (400MHz, D_2O): δ [ppm] = 4.11 (t, J = 6.4 Hz, 1H), 2.42 – 2.36 (m, 2H), 2.36 (s, 1H), 2.19 – 2.10 (m, 1H), 2.07 – 1.98 (m, 1H); 13C NMR (101MHz, D2O): δ 82.28, 71.16, 52.05, 28.44, 14.16; HRMS (ESI): $C_6H_9NO_2$ $[M+H]^+$ 128.06, found 128.07; $[\alpha]_{20}^{D}$: +32.4 (c = 1, 1 M HCl); Ref [76]: +28 (c = 1, 1 M HCl).

Bacterial culture, metabolic labeling and viability assessment based on growth rate

Mycobacterium tuberculosis (*Mtb*) strain H37Rv, expressing DsRed from a pSMT3[Phsp60/DsRed] plasmid[50], was cultured in Difco Middlebrook 7H9 broth with 10% ADC, 0.05% Tween-80, 0.2% glycerol and 50 µg/mL hygromycin B (Thermo Fisher Scientific) shaking at 37°C. Fresh cultures were inoculated from glycerol stocks every 2 months due to loss of DsRed expression over time. For metabolic labeling of *Mtb*, cultures were supplemented with 4 mM Hpg, 4 mM Aha, 5 mM alkDala or a combination of 4 mM Aha and 5 mM alkDala ('dual') and incubated

under normal culturing conditions. After 0h, 8h, 24h, 48h, 72h and 144h, bacterial growth was assessed by OD_{600} measurement and normalized on the first time point to determine the growth rate in the presence or absence of metabolic labels. These growth rates were plotted as percentages of the unlabeled *Mtb* control culture. After the last time point, the bacteria were collected by centrifugation (15 min at 3200 rcf) and resuspended in fresh 7H9 to assess the bacterial growth recovery after label incorporation, over another incubation period of 144h.

Mammalian cell culture and infection experiments

RAW 264.7 cells (ATCC TIB-71), a mouse monocyte/macrophage cell line, were cultured in DMEM (Sigma-Aldrich) supplemented with 10% FCS, GlutaMAX, penicillin 100 I.U./mL and streptomycin 50 µg/mL and incubated at 37°C, 5% CO_2. For infection experiments, 10 million cells were seeded on a 10 cm dish for each condition in minimal medium (DMEM, 10% FCS, GlutaMAX), allowed to attach for 8 hours and pre-stimulated with 25 ng/mL LPS-B4 (Sigma-Aldrich) for an additional 18 hours. Cells were infected with triple label *Mtb* at an MOI of 25 for 1 hour, washed three times with minimal medium containing 30 µg/mL gentamicin and incubated for 24 hours, in the presence or absence of 5 µg/mL gentamicin. For intracellular treatment with antibiotics, 1 µg/mL (1.2 µM) rifampicin, 2 µg/mL (14.6 µM) isoniazid, 5 µg/mL (18.0 µM) ethambutol or a combination of the three ('triple-antibiotics cocktail'), was added to the medium during the 24-hour incubation post-infection. For *in vitro Mtb* treatment with antibiotics, triple label *Mtb* were incubated for 24 hours in minimal cell medium containing the triple-antibiotics cocktail, washed once with fresh minimal cell medium and subsequently added to the cells for 1 hour to allow phagocytosis (infection).

Analysis of label incorporation by in-gel fluorescence

Mtb expressing DsRed were metabolically labeled as described above and samples of $OD_{600} \approx 0.5$ were collected after 8h, 24h and 48h to analyze the label incorporation levels into the bacterial proteome, by in-gel fluorescence. Bacterial samples were pelleted by centrifugation (10 min at 9000 rcf), washed once with PBS and resuspended in 100 µL lysis buffer. Lysis buffer and conditions were varied (**Table 1**) to allow for optimal killing and recovery of bacterial proteins, while maintaining compatibility with subsequent copper(I)-catalyzed Huisgen cycloaddition (ccHc or 'click') reaction. Optimal lysis and protein recovery was achieved with 1% SDS and immediate heat treatment (30 min at 80°C). Protein concentration of the lysates was determined using Qubit Protein Assay (Thermo Fisher Scientific) and 10 µg protein was diluted to 20 µL total volume. Lysates were

reacted with AF647-azide (Hpg/alkDala) or alkyne (Aha/dual) by ccHc, through direct addition of 10 µL 3X concentrated 'click cocktail' (3 mM copper sulfate, 30 mM sodium ascorbate, 3 mM THPTA ligand, 30 mM aminoguanidine, 100 mM HEPES pH 8 and 15 µM fluorophore; mixed in this exact order) and incubated for 1 hour at room temperature. The reaction was quenched by adding 10 µL 4X concentrated Laemmli sample buffer and boiling for 5-10 min at 95°C, followed by brief cooling on ice. 10 µL of the fluorophore-labeled lysates was loaded on a 15-slot 12.5% gel and separated by SDS-PAGE. In-gel fluorescence was measured on a Bio-Rad Chemidoc MP Imaging System (Bio-Rad Laboratories), followed by Coomassie Brilliant Blue staining and imaging as a protein loading control. Gel images were analyzed with Bio-Rad Image Lab Software (Bio-Rad Laboratories).

Analysis of label incorporation by flow cytometry

Mtb expressing DsRed were metabolically labeled as described above and samples of OD_{600} ≈ 0.5 were collected after 8h, 24h and 48h to analyze the label incorporation levels per bacterium, by flow cytometry. Bacterial samples were pelleted by centrifugation (10 min at 9000 rcf), washed once with PBS and resuspended in 100 µL fixative. Fixation and permeabilization conditions were varied (**Table 2**) to allow for optimal penetration of click fluorophores into the fixed bacteria, to reach the targeted bioorthogonal labels. Washing conditions were varied (**Table 3**) to allow for optimal resuspension and recovery of fixed bacteria, using an anti-clumping additive. Optimal fluorophore penetration and recovery of fixed bacteria were achieved by pre-permeabilizing the bacteria with 1% SDS in PBS for 15 min at room temperature, followed by fixation with 4% paraformaldehyde in PBS for 24 hours at room temperature, after collecting the bacteria by centrifugation (10 min at 9000 rcf). Fixed bacteria were collected by low-speed centrifugation (10 min at 2000 rcf) and stored in 0.5% paraformaldehyde in PBS at 4°C until all time points were collected. Low-speed centrifugation was used to collect the fixed bacteria in between all further steps, to avoid damage due to excessive G-forces. Bacteria were washed once with PBS to remove residual paraformaldehyde and once with FACS buffer (0.1% BSA, 20 mM glycine in PBS) to quench free aldehydes. The first ccHc reaction, with AF647-azide, was performed, by resuspending the bacteria in 'click cocktail' (1 mM copper sulfate, 10 mM sodium ascorbate, 1 mM THPTA ligand, 10 mM aminoguanidine, 100 mM HEPES pH 8 and 5 µM fluorophore; mixed in this exact order), and incubating for 1 hour at room temperature. After a single wash with FACS buffer, the second ccHc reaction, with AF488-alkyne, was performed in the same manner. After another wash with FACS buffer, the bacteria were resuspended in blocking buffer (1% BSA, 10 mM EDTA in

PBS) and incubated for 30 min at room temperature, to assist the removal of non-specifically bound fluorophores. After a final wash with FACS buffer, the bacteria were resuspended in FACS buffer and measured on a BD FACSLyric Flow Cytometer (BD Biosciences). The UV-autofluorescence of *Mtb* was detected in the V450 channel, Aha-AF488 was detected in the FITC channel, DsRed was detected in the PE channel and alkDala-AF647 was detected in the APC channel. Automatic compensation was provided by the integrated BD FACSuite software (BD Biosciences) and all subsequent analysis was performed with FlowJo V10 (FlowJo software). The measured events were gated on size, shape and fluorescence to accurately select single bacteria (Fig. 2A). Quantification of label incorporation was achieved by selecting the median fluorescence intensity (MFI) of the major [Aha+/alkDala+] population for dually-labeled *Mtb* or the major [Aha-/alkDala-] population for unlabeled *Mtb* (Fig. 2A, Fig. S2).

Preparation of single-bacteria samples for CLEM

Mtb expressing DsRed were metabolically labeled as described above and samples of 50 mL were collected after 1h, 24h and 48h to analyze the label incorporation levels into the bacterial proteome and cell wall, by on-section ccHc reaction. Unlabeled control bacteria were included as a control for background fluorescence of on-section ccHc reaction. Bacteria were collected by centrifugation (15 min 3000 rcf), washed once with PBS and resuspended in a fixation solution optimized for Transmission Electron Microscopy (TEM) (2% EM-grade paraformaldehyde, 0.2% EM-grade glutaraldehyde in 0.1M phosphate buffer pH 7.2) and rotated for 2 hours at room temperature. The fixed bacteria were collected by centrifugation and stored in storage buffer (0.5% EM-grade paraformaldehyde in 0.1M phosphate buffer pH 7.2) at 4°C until all time points were collected. The fixed bacteria were washed with PBS and aldehyde residues were quenched with 20 mM glycine in PBS. Next, the bacteria were collected by centrifugation, resuspended in warm 1% gelatin in PBS, transferred to a 1.5 mL Eppendorf tube, resuspended in warm 12% gelatin in PBS and pelleted by centrifugation (3 min at 5000 rcf). After jellification on ice, the sample pellet was cut off from the tube and cut in half with a razor knife. Sample cubes of approx. 1 mm^2 were prepared and rotated in a 2.3 M sucrose solution for 18 hours to allow for sucrose infiltration, as a cryo-protectant, followed by plunge-freezing the cubes on metal support pins.

Preparation of *Mtb*-infected macrophage samples for CLEM

Following infection and post-infection incubation of triple labeled *Mtb* in RAW 264.7 cells, in the presence or absence of antibiotics, the cells were washed three

times with minimal cell medium containing 30 µg/mL gentamicin and once with PBS. The cells were fixed with TEM-optimized fixation solution (2% EM-grade paraformaldehyde, 0.2% EM-grade glutaraldehyde in 0.1M phosphate buffer pH 7.2) for 2 hours at room temperature, rinsed with PBS and stored in storage buffer (0.5% EM-grade paraformaldehyde in 0.1M phosphate buffer pH 7.2) at 4°C until all time points were collected. Fixed cells were rinsed with PBS, harvested in warm 1% gelatin in PBS with cell scrapers and transferred to a 15 mL Falcon tube. The cells were collected by centrifugation, resuspended in warm 1% gelatin in PBS, transferred to a 1.5 mL Eppendorf tube, resuspended in warm 12% gelatin in PBS and pelleted by centrifugation (3 min at 800 rcf). Samples were further processed for plunge-freezing as described for the bacteria-only samples above.

Cryo-sectioning and on-section ccHc reaction

Ultrathin (75 nm) cryo-sections were prepared according to the Tokuyasu technique [54,55], using a cryo-ultramicrotome (Leica) and diamond knife (Diatome). Sections were thawed on a droplet of pickup fluid (1.15 M sucrose, 1% methylcellulose) and transferred to a Formvar/carbon-coated TEM grid (titanium, 100 square mesh, 3.05 mm, center-marked; Agar Scientific), pre-coated with blue 0.2 µm FluoSpheres (Thermo Fisher) as fiducial markers. Thawed cryo-sections attached to the TEM grid were incubated on 2% gelatin in PBS for 30 min at 37°C, followed by washing on 20 mM glycine in PBS (5x 2 min). Next, the sections were subjected to ccHc reaction with AF647-azide (or AF647-alkyne for analysis of label incorporation) on a droplet of 'click cocktail' (1 mM copper sulfate, 10 mM sodium ascorbate, 1 mM THPTA ligand, 10 mM aminoguanidine, 100 mM HEPES pH 8 and 5 µM fluorophore; mixed in this exact order), for 1 hour at room temperature. After several washes with PBS, the second ccHc reaction with AF488-alkyne was performed, followed by several washed with PBS. The sections were then incubated on droplets of 1% BSA in PBS for 3 x 10 min at room temperature, to assist the removal of non-specifically bound fluorophores. Nuclear staining of the host cells was achieved by incubating the sections on a droplet of 0.2 µg/mL DAPI in PBS for 5 min.

Confocal microscopy

After several washes with PBS, the fluorescently-labeled sections attached to TEM grids were mounted in water containing 30% glycerol between a microscopy slide and a coverslip, and sealed with silver Scotch tape. The samples were imaged on an Andor Dragonfly 505 Spinning Disk Confocal (Oxford Instruments), containing an 8-line integrated laser engine, on a Leica DMi8 inverted microscope equipped with a

100X/1.47 HC PL APO TIRF-corrected oil objective. FluoSpheres were excited with the 405 line and collected with the 450/50 BP emission filter, AF488 was excited with the 488 line and collected with the 525/50 BP emission filter, DsRed was excited with the 561 line and collected with the 620/60 BP emission filter and AF647 was excited with the 637 line and collected with the 700/75 BP emission filter. Images were acquired with the Zyla 2048x2048 sCMOS camera and 2x2 camera binning controlled with the integrated Fusion software. Z-series optical sections were collected with a system-optimized step-size of 0.13 microns and deconvolved using the integrated ClearView-GPU™ deconvolution software. Z-series are displayed as maximum z-projections, and gamma, brightness and contrast were carefully adjusted (identically for compared image sets) using FIJI.[77] Maximum intensity projections were made, in order to compensate for non-flat sections.

TEM imaging and correlation

After acquiring the fluorescence microscopy (FM) images, the TEM grids containing the sections were recovered from the microscopy slides, rinsed in distilled water and incubated for 5 min on droplets of uranyl acetate/methylcellulose. The negatively-stained sections were then imaged on a FEI Tecnai 12 BioTwin TEM System (FEI Technologies) at 120 kV acceleration voltage. Correlation of FM and TEM images was performed in Adobe Photoshop CC 2020 (Adobe Systems). The separate fluorescence channels were imported as layers, set to overlay mode 'Lighten', then grouped and set to overlay mode 'Color', placed on top of the TEM image. Transformation of the FM image to match the TEM image was achieved by isotropic scaling with interpolation setting 'bicubic smoother', translation and rotation. Alignment at low magnification was guided by the grid bars and sample shape for single bacteria or nuclei for *Mtb*-infected cells. Alignment at high magnification was guided by the fiducial beads and the position of the bacteria. Minor manual corrections for chromatic aberration were applied where required, guided by the obvious bacterial shapes, showing a clear internal [DsRed+/Aha+] part and a ring-like [alkDala+] cell wall.

Quantification of intracellular *Mtb* localization and shape *in situ* by CLEM-based data analysis

The intracellular localization and shape of triple label *Mtb*, in the presence or absence of antibiotics, was quantified by manual counting of bacteria in the large CLEM image, using Adobe Photoshop CC 2020 (Adobe Systems). Fluorescence was used to guide the detection of bacteria, and the geometrical shapes tool ('rectangle', 'rounded rectangle', 'ellipse', 'polygon' and 'custom shape') was used

to classify bacteria and host cells based on their appearance and localization, which allowed for facile automatic counting for each of the categories (geometric shapes) by Photoshop. The complete large field of view CLEM image was used for quantification, which allowed for a large data set of over 500 bacteria per condition. The distribution of intracellular bacteria was classified as either 'no vacuole', 'small/tight vacuole' or 'large/spacious vacuole' to allow unbiased counting, and plotted as percentage relative to the total number of intracellular bacteria counted. Extracellular bacteria were counted separately and plotted as percentage relative to the total number of intracellular and extracellular bacteria counted. The appearance (bacterial profile) of intracellular bacteria was classified as either 'regular shape' or 'irregular shape' to allow unbiased counting, and plotted as percentage relative to the total number of bacteria counted. Host cell death was quantified by counting disintegrated cell profiles, still containing a DAPI-positive compartment to allow unbiased counting, and plotted as percentage relative to the total number of nucleus-containing cell profiles counted. Each of the conditions was tested at least twice but the quantified data were obtained from a single experiment in which all conditions were tested simultaneously in parallel, to avoid technical variations.

Quantification of intracellular *Mtb* size and label retention *in situ* by CLEM-based data analysis

Label retention of intracellular triple label *Mtb*, in the presence or absence of antibiotics, was quantified by semi-automatic analysis of the fluorescence (DsRed, Aha-AF488, alkDala-AF647). To this end, a JavaScript was created using the Adobe Photoshop CC Script Listener Plug-in for Windows (2020 version, downloaded from https://helpx.adobe.com/photoshop/kb/downloadable-plugins-and-content.html), in combination with some manual modifications, and is freely available upon request. The resulting script only requires manual selection of the outline of a bacterium using the 'lasso tool', and allows for automatic cropping of the selected bacterium, followed by removal of the external area surrounding the outline. The bacterial fluorescence profiles for each channel (as well as the TEM image) are exported separately and saved as TIF files in a '[channel]_bacterium_[number]' format that allows automatic pairing and counting. A secondary ImageJ (IJ1) Macro-style script was created to automatically analyze all exported bacterial fluorescence profiles, based on average fluorescence intensity, and is freely available upon request. The resulting data points were plotted individually in violin plots using GraphPad Prism 8 (GraphPad Software). Each of the conditions was tested at least twice but the

quantified data were obtained from a single experiment in which all conditions were tested simultaneously in parallel, to avoid technical variations.

Quantification of *Mtb* label retention by flow cytometry after recovery from host cell (*ex cellula*)

Following infection and post-infection incubation of triple labeled *Mtb* in RAW 264.7 cells, in the presence or absence of antibiotics (identical to CLEM experiment), the cells were washed three times with minimal cell medium containing 30 µg/mL gentamicin and once with PBS. Cells were lysed with lysis buffer (0.1% Triton-X100, 150 mM NaCl, 20 mM Tris-HCl) for 15 min at room temperature and the cell debris was separated from the bacteria by centrifugation (5 min at 600 rcf) and pellet discarded. The bacteria were collected by centrifugation (15 min at 3000 rcf), pre-permeabilized with 1% SDS in PBS and fixed with 4% paraformaldehyde in PBS for 24 hours at room temperature. Fixed bacteria were collected by low-speed centrifugation (10 min at 2000 rcf) and stored in 0.5% paraformaldehyde in PBS at 4°C until all time points were collected. The isolated bacteria were further processed and measured by flow cytometry, as described for the freshly labeled *Mtb* above. The measured events were gated on size, shape and fluorescence to accurately select single bacteria (Fig. 2A). Quantification of label retention was achieved by selecting the MFI of the major [Aha+/alkDala+] population and corresponding [autofluorescence+/DsRed+] population (Fig. 6B, Fig. S12). Each of the conditions was tested at least twice but the quantified data were obtained from a single experiment in which all conditions were tested simultaneously in parallel, to avoid technical variations.

Statistics

The unpaired two-tailed Mann-Whitney U test and Chi-Square (χ^2) test were performed using GraphPad Prism 8 (GraphPad Software). The Benjamini-Hochberg procedure for multiple testing was performed in Microsoft Excel 2016 (Microsoft), with a False Discovery Rate (FDR) of 0.1.

5.5 Supplemental Figures

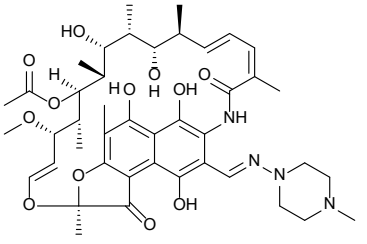

Rifampicin

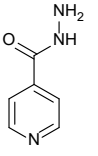

Isoniazid

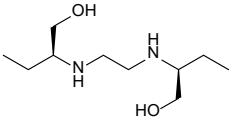

Ethambutol

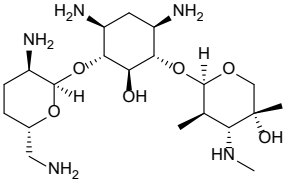

Gentamicin

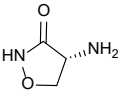

D-cycloserine

Figure S1. Overview of antibiotics used in this study. Rifampicin is a polyketide antibiotic that inhibits bacterial RNA synthesis by binding to the RNA polymerase β subunit.[78] Isoniazid is a prodrug that is activated by KatG to form a nicotinoyl-NAD adduct, which in turn inhibits mycolic acid synthesis, thereby interfering with the mycobacterial cell wall synthesis.[79] Ethambutol is a small molecule antibiotic that inhibits arabinogalactan synthesis, thereby interfering with the bacterial cell wall synthesis.[80] The bacteriostatic and/or bactericidal effect of these antibiotics are concentration-, time- and growth phase dependent, and may differ when used in combination.[81,82] Gentamicin is a bactericidal aminoglycoside antibiotic that inhibits bacterial protein synthesis by binding to the bacterial ribosome.[83] Gentamicin is not cell permeable but is actively taken up by Gram-negative bacteria in an oxygen-dependent manner.[84] D-cycloserine is a cyclic D-alanine analogue that blocks peptidoglycan synthesis, thereby interfering with the bacterial cell wall synthesis.[85] D-cycloserine can be bacteriostatic or bactericidal depending on the concentration and the susceptibility of the bacterial species.[86]

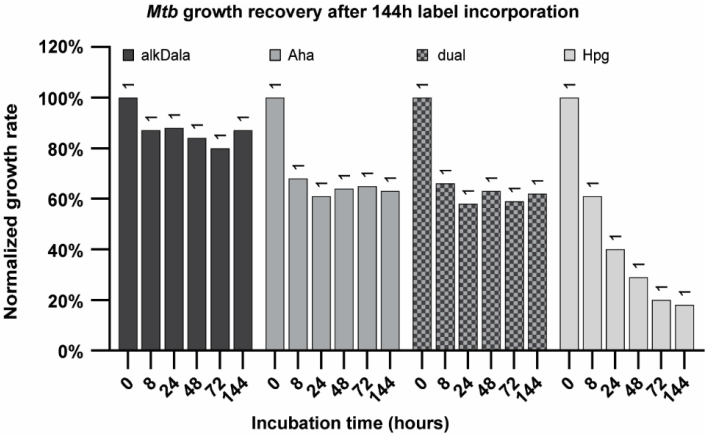

Figure S2. Growth recovery of *Mtb* after 144h label incorporation relative to control. DsRed-expressing *Mtb* H37Rv were first incubated with 4 mM Hpg, 4 mM Aha, 5 mM alkDala or a combination of 4 mM Aha and 5 mM alkDala (dual), for 144h in Middlebrook 7H9 broth (shown in Fig. 1A). The medium was then replaced by fresh 7H9 broth without metabolic labels and the bacterial growth recovery after labeling was assessed for another 144h by OD_{600} measurements, normalized on the first time point. The number of biological replicates for each OD_{600} measurement is indicated above the bar.

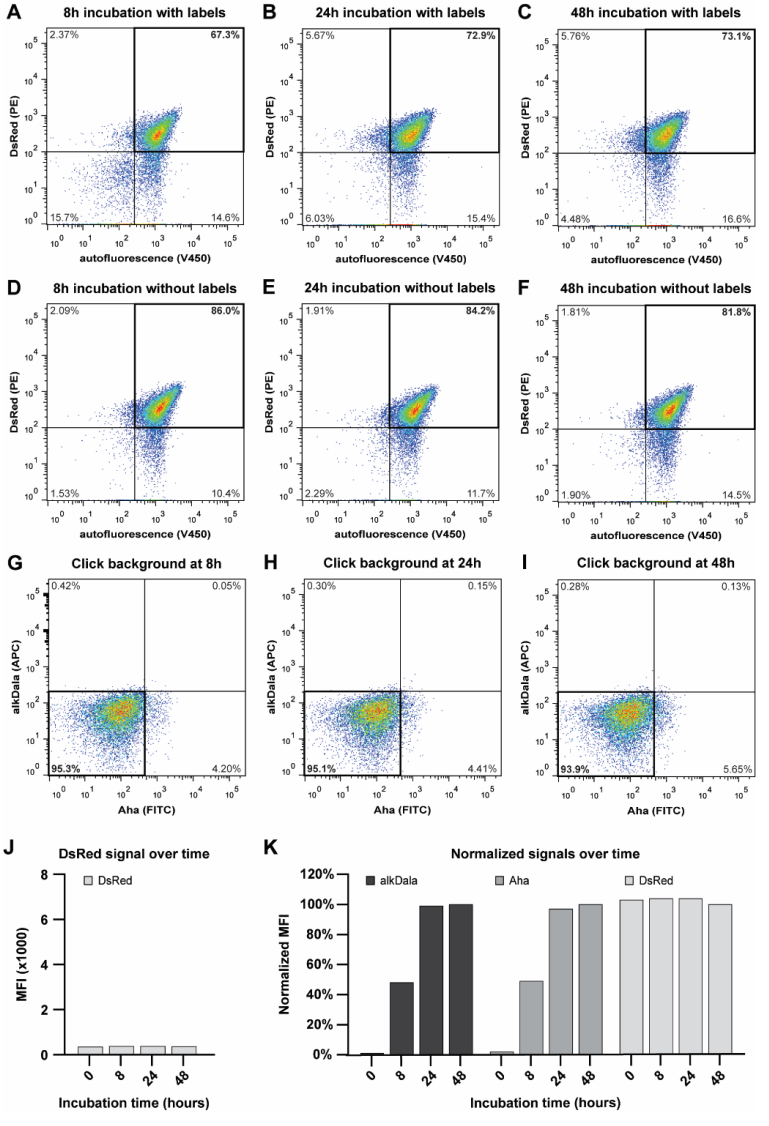

Figure S3. Controls of label incorporation over time by flow cytometry. DsRed-expressing *Mtb* H37Rv were incubated with a combination of 4 mM Aha and 5 mM alkDala or without labels, for the indicated time in Middlebrook 7H9 broth. Bacterial samples of 0.5 OD were collected, pre-permeabilized with 1% SDS and fixed in 4% paraformaldehyde. Fixed and permeabilized bacteria were reacted with AF647-azide (alkDala) and AF488-alkyne (Aha) by two sequential ccHc reactions. The effect of label incorporation on DsRed fluorescence was assessed after 8 h (**A**), 24 h (**B**) and 48 h (**C**) incubation and compared to incubation without metabolic labels after 8 h (**D**), 24 h (**E**) and 48 h (**F**). The background fluorescence of the ccHc (click) reaction was analyzed after incubation without metabolic labels for 8 h (**G**), 24 h (**H**) and 48 h (**I**). **J:** The effect of label incorporation on DsRed fluorescence over time is shown as the median fluorescence intensity (MFI), on the same scale as used in Fig. 2A for comparison. **K:** The relative change in label incorporation over time and the resulting effect on DsRed fluorescence are shown as normalized MFI values, corresponding to the MFI values presented in Fig. 2A and panel **J** of this figure.

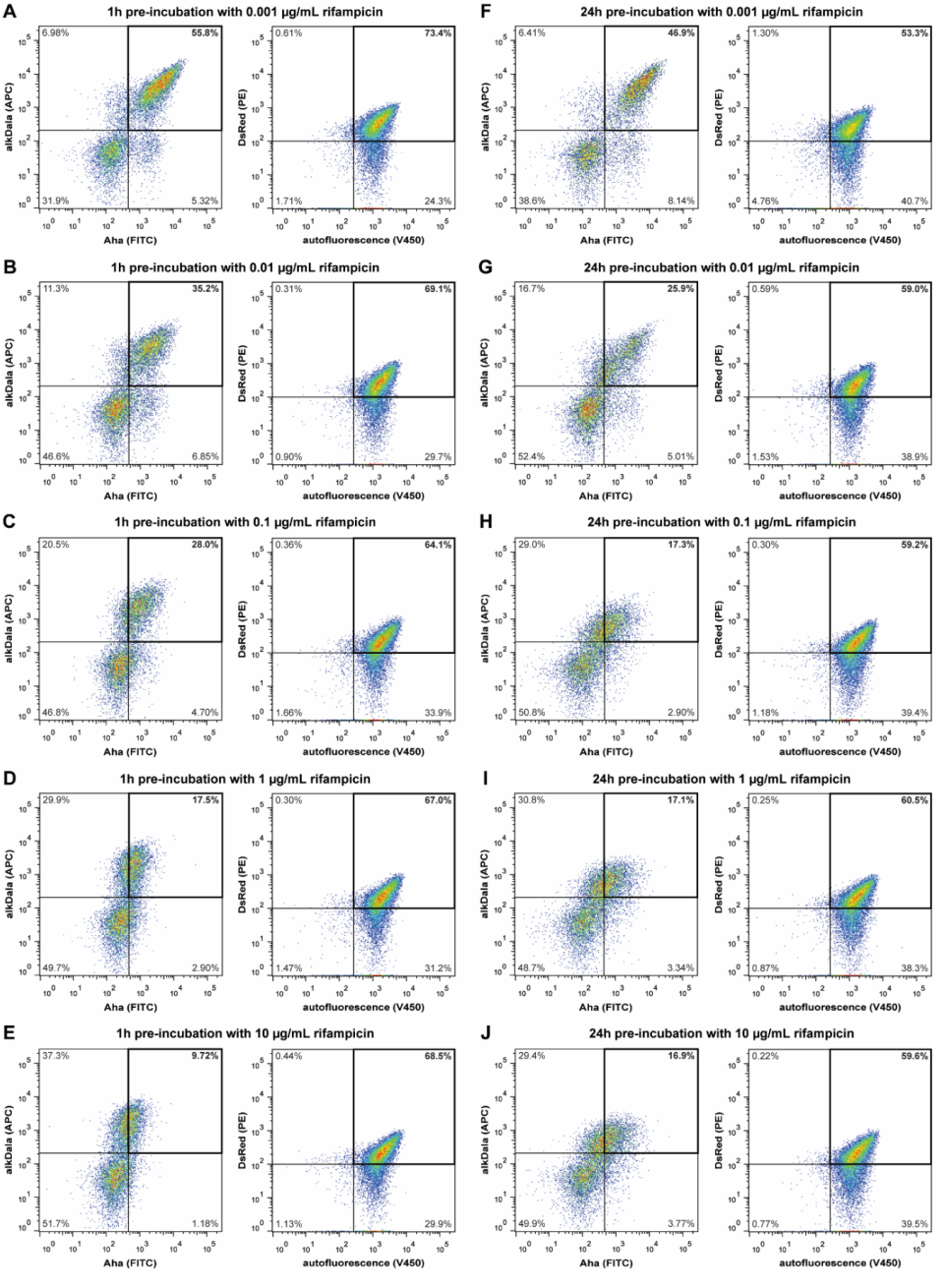

Figure S4. Controls of label incorporation over time by flow cytometry in presence of increasing concentrations of Rifampicin. DsRed-expressing *Mtb* H37Rv were cultured and analyzed as for Figure S2 after pretreatment with for either 1h (**A-E**) or 24h (**F-J**) with rifampicin in increasing concentrations.

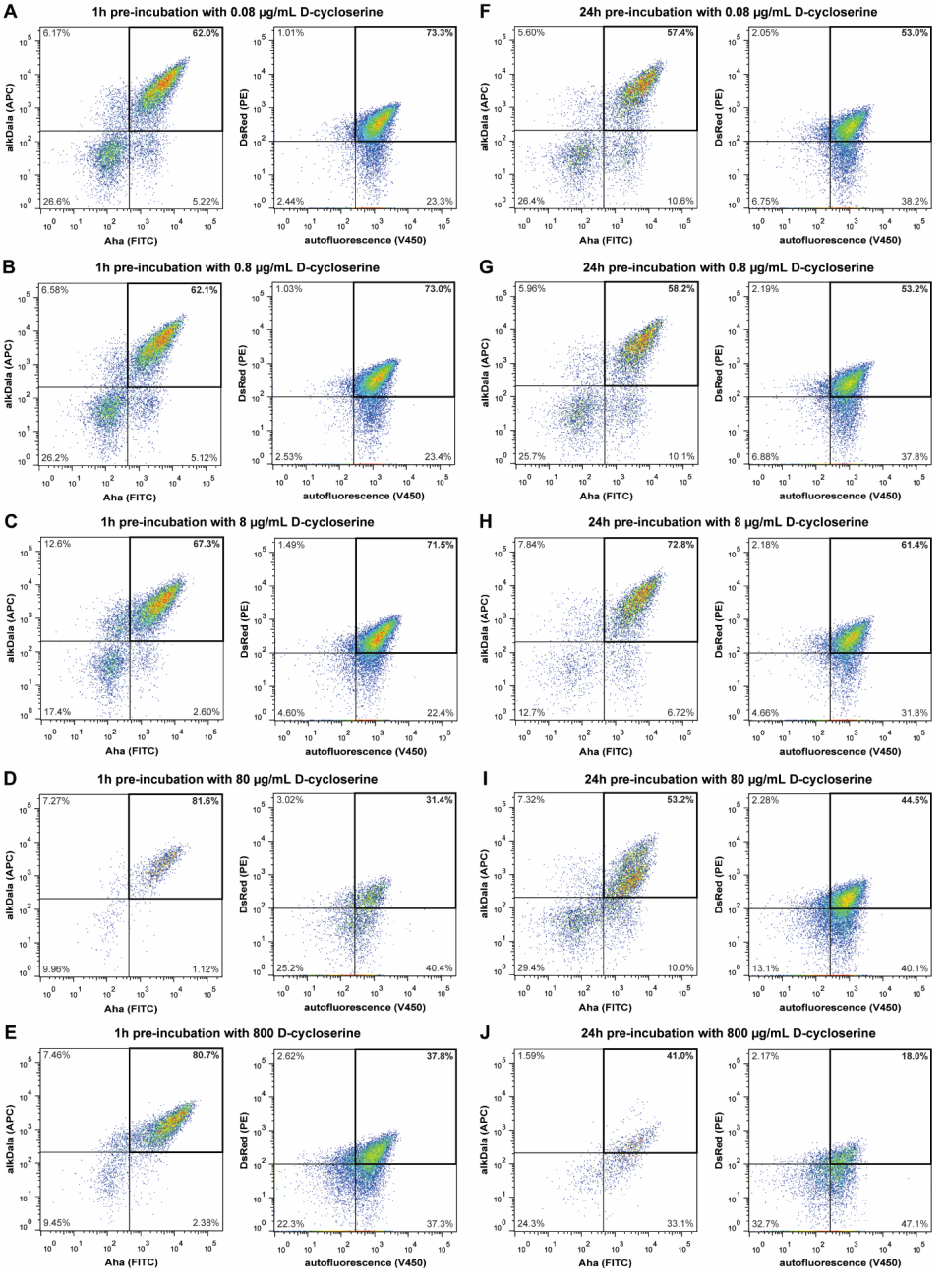

Figure S5. Controls of label incorporation over time by flow cytometry in presence of increasing concentrations of D-cycloserine. DsRed-expressing *Mtb* H37Rv were cultured and analyzed as for Figure S2 after pretreatment with for either 1h (**A-E**) or 24h (**F-J**) with D-cycloserine in increasing concentrations.

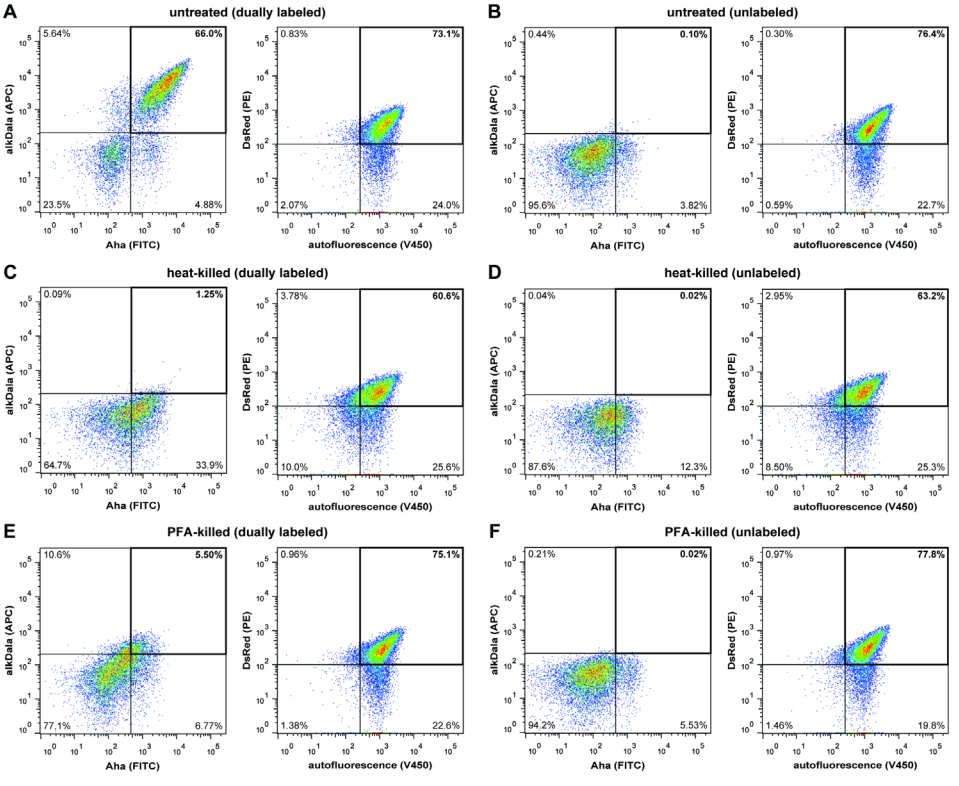

Figure S6. Controls of label incorporation by flow cytometry after heat-killing or PFA-fixation. **A/B:** Untreated control bacteria with or without metabolic labels. **C/D:** Heat-killed bacteria (30 min at 80 °C) with or without metabolic labels. **E/F:** PFA-killed bacteria (30 min in 4% PFA) with or without metabolic labels.

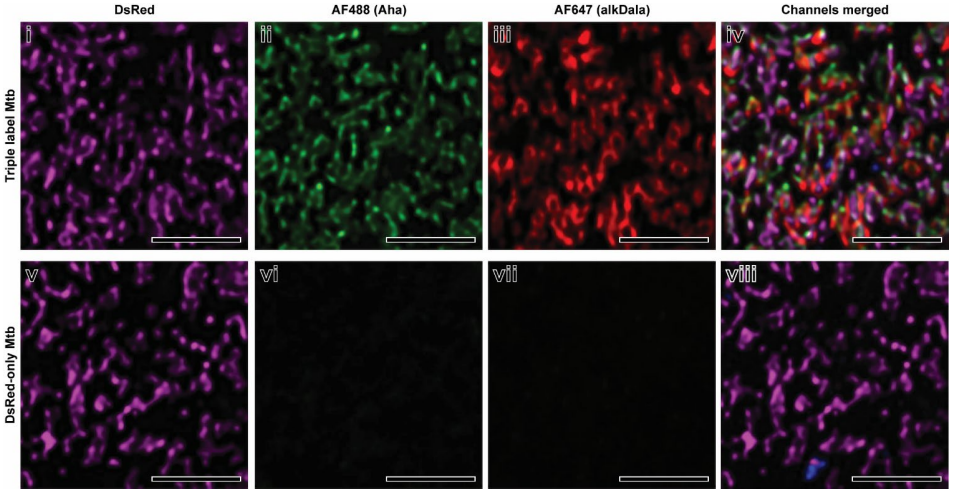

Figure S7. Signal and background fluorescence of on-section click reactions. Triple label *Mtb* and DsRed-only *Mtb* were prepared, followed by cryo-sectioning and dual on-section ccHc reaction with AF647-azide (alkDala) and AF488-alkyne (Aha), sequentially. The resulting confocal microscopy images are shown as separated fluorescence channels for clarity. All scale bars represent 5 µm.

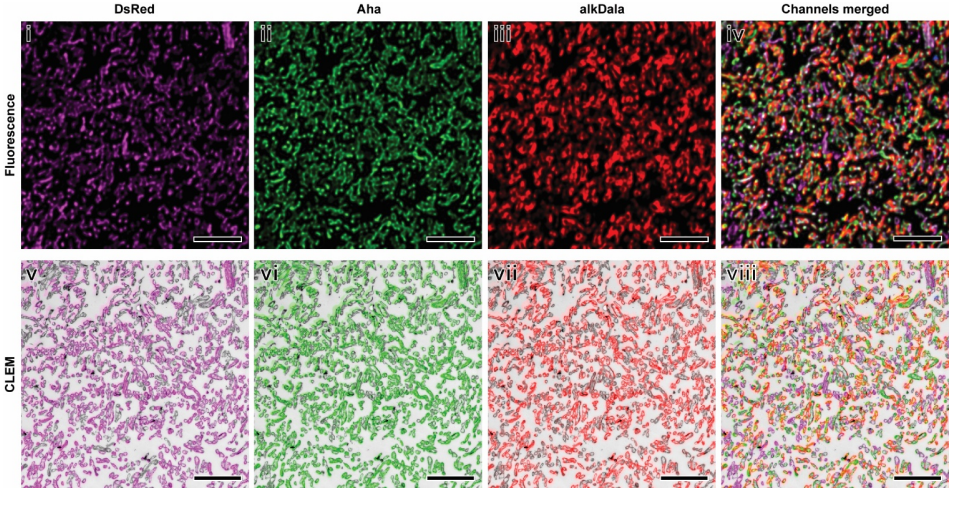

Figure S8. Large area CLEM image of *Mtb in vitro*, corresponding to the details presented in Fig. 3. Triple label *Mtb* and DsRed-only *Mtb* were prepared and subsequently prepared for cryo-sectioning, followed by cryo-sectioning and dual on-section ccHc reaction with AF647-azide (alkDala) and AF488-alkyne (Aha), sequentially. The sections were imaged by confocal microscopy, then stained with uranyl acetate and imaged by TEM. The resulting fluorescence and TEM images were correlated in Photoshop to obtain the CLEM image, shown in the bottom panel. The top panel shows the corresponding fluorescence channels separately for clarity. All scale bars represent 5 µm.

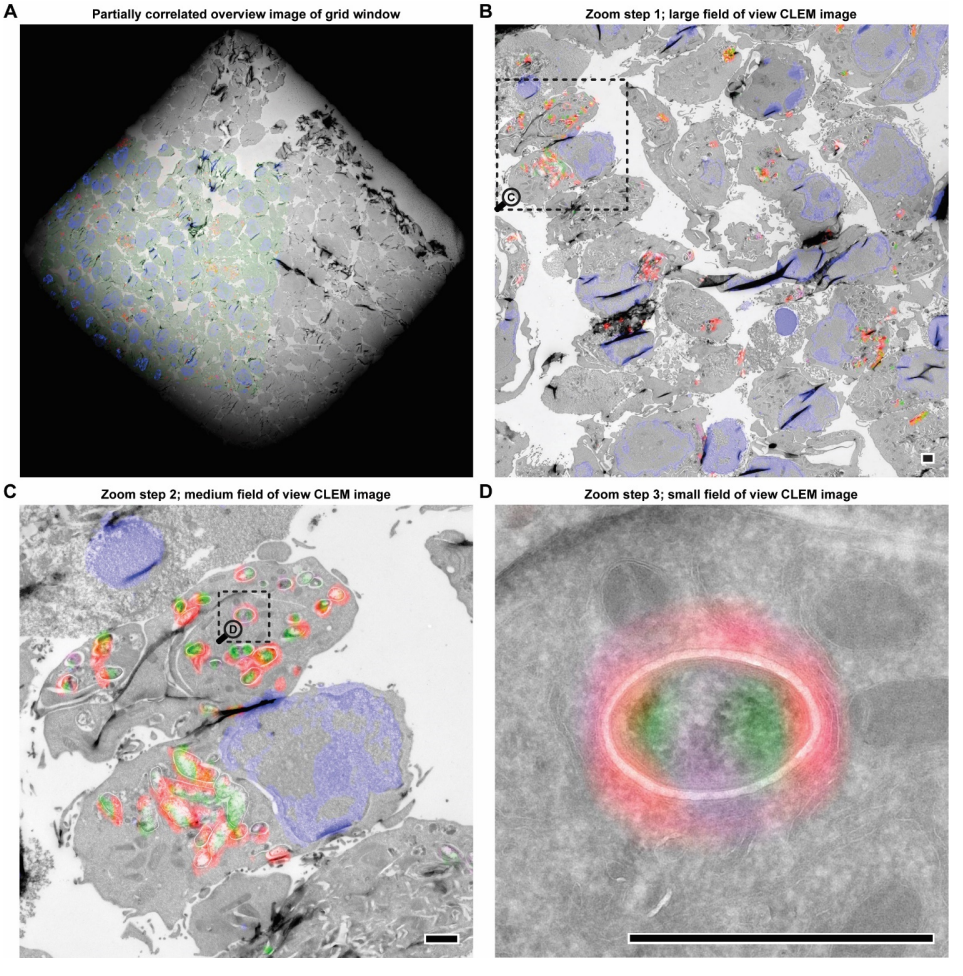

Figure S9. Stepwise zooming in from an ultra large field of view CLEM image, corresponding to the details presented in Fig. 4. RAW 264.7 macrophages were infected with triple label *Mtb*, incubated for 24 hours without antibiotics, and subsequently prepared for cryo-sectioning, followed by dual on-section ccHc reaction with AF647-azide and AF488-alkyne. The resulting confocal fluorescence image was correlated onto the corresponding large field of view (stitched) TEM image, using Photoshop. An entire window in the TEM grid could be partially correlated with the available fluorescence image, depending on the orientation of the grid during acquisition (**A**). Photoshop allows zooming to an area of interest to provide the required details, while keeping the channels separated (i.e. multimodal dataset). The boxed area in the large field of view CLEM image (**B**) corresponds to the medium field of view image (**C**), in which the boxed area corresponds to the small field of view image (**D**; separated channels shown in Fig. 4i-iv). All scale bars represent 1 µm.

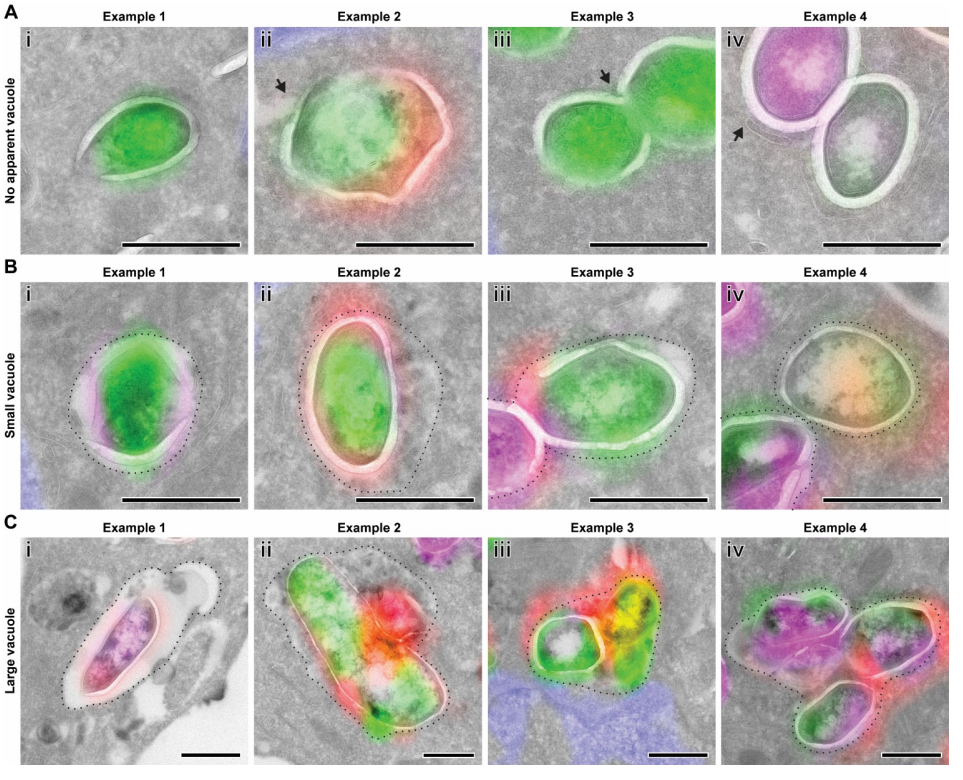

Figure S10. *Mtb* displays a heterogeneous intracellular distribution in host cells. RAW 264.7 macrophages were infected with triple label *Mtb* and incubated with or without antibiotics, and subsequently prepared for cryo-sectioning, followed by dual on-section ccHc reaction with AF647-azide and AF488-alkyne. The resulting confocal fluorescence image was correlated onto the corresponding large field of view (stitched) TEM image, using Photoshop. A small percentage of bacteria appears to have escaped into the cytosol, as no vacuole can be observed (**A**). These bacteria may fuse again with a vacuole (**ii**), divide cytosolically (**iii**) or potentially be re-compartmentalized into a double membrane autophagosome (**iv**). An intermediate percentage of bacteria resides in a small vacuole (**B**), that can appear empty (**i**) or filled with smaller vacuoles/granules (**ii**). Bacteria may divide within small vacuoles (**iii**) and the vacuole may wrap tightly around the bacterium (**iv**). A large percentage of bacteria resides in large vacuoles (**C**) that may appear spacious (**i**) or filled with smaller vesicles/granules (**ii**). Vacuoles containing a cluster of bacteria were classified as large, regardless of being smaller (**iii**) or larger (**iv**). A dotted line indicates the apparent vacuole where relevant. All scale bars represent 500 nm.

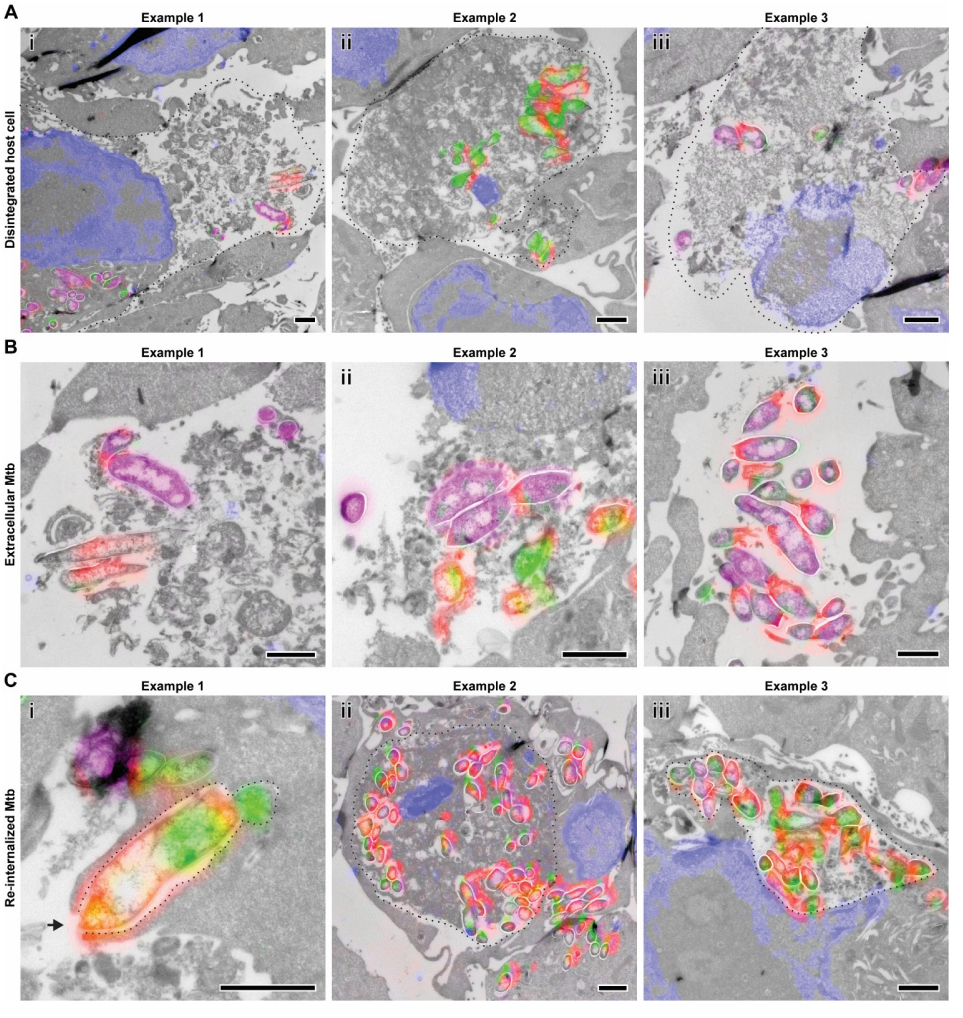

Figure S11. *Mtb* is released from host cell and subsequently re-internalized by surrounding macrophages. RAW 264.7 macrophages were infected with triple label *Mtb* and incubated with or without antibiotics. The resulting confocal fluorescence image was correlated onto the corresponding large field of view (stitched) TEM image, using Photoshop. Some *Mtb*-containing macrophages are disintegrated (**A**), probably as a result of the *Mtb* infection**.** The escaped bacteria reside extracellularly (**B**), surrounded by cell debris. Extracellular bacteria appear to be re-internalized by neighboring cells (**C**), through phagocytosis of separate bacteria (**i**) or internalization of the entire necrotic cell (**ii**), which can result in large vacuoles that contain both bacteria and cell debris (**iii**). A dotted line indicates the apparent cell outline or vacuole where relevant. All scale bars represent 1 µm.

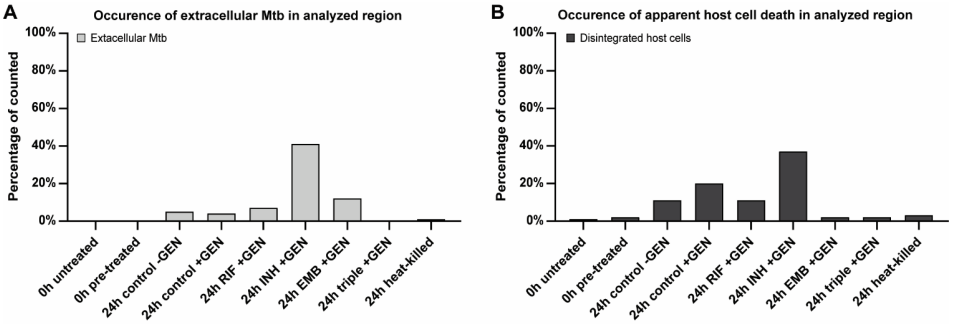

Figure S12. The occurrence of extracellular *Mtb* and apparent host cell death changes upon treatment with antibiotics. RAW 264.7 macrophages were infected with triple label *Mtb* for 1 hour and immediately analyzed (0h untreated) or further incubated for 24 hours with rifampicin (RIF), isoniazid (INH), ethambutol (EMB), a combination of the three (triple) or no antibiotics (24h control) and compared to *Mtb* pre-treated with triple antibiotics before infection (0h pre-treated). An additional control with heat-killed *Mtb* (prior to infection) was included as a negative control for pathogenicity. **A:** *Mtb* in the absence of host cell or inside a disintegrating host cell were classified as extracellular *Mtb*. Shown as percentage relative to total number of *Mtb* counted in the analyzed region; n>500 bacteria counted. **B:** Disintegrating and/or entirely phagocytosed macrophages were classified as host cell death. Shown as percentage relative to total number of macrophages counted in the analyzed region; n>80 cells counted.

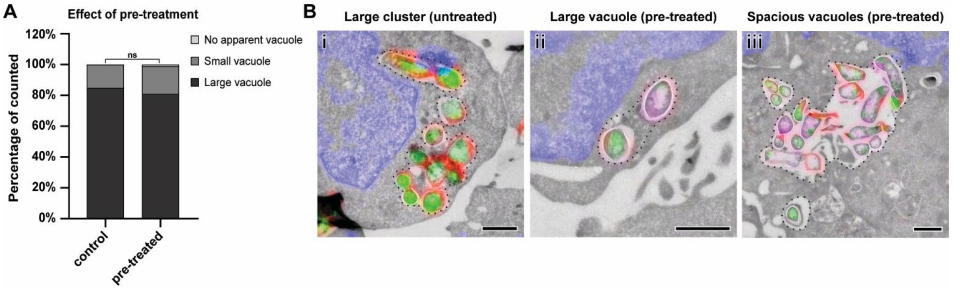

Figure S13. *Mtb* resides primarily in large vacuoles directly after infection. RAW 264.7 macrophages were infected with triple label *Mtb* for 1 hour with viable *Mtb* (0h control) or *Mtb* pre-treated with rifampicin, isoniazid and ethambutol (0h pre-treated), and analyzed immediately after infection. The resulting confocal fluorescence image was correlated onto the corresponding large field of view (stitched) TEM image, using Photoshop. **A:** Intracellular distribution of *Mtb* was manually classified as no vacuole/cytosolic (none), small/tight vacuole (small) or large/spacious vacuole (large). Shown as percentage relative to total number of intracellular *Mtb* counted in the analyzed region; n>200 bacteria counted. **B:** Most untreated bacteria reside in large clusters of smaller vacuoles (**i**), that were considered large vacuoles for unbiased counting, while most of the pre-treated bacteria reside in large (**ii**) and spacious (**iii**) vacuoles. This distinction was not considered in the quantification in order to avoid interpretation bias. A dotted line indicates the apparent vacuole where relevant. All scale bars represent 1 µm.

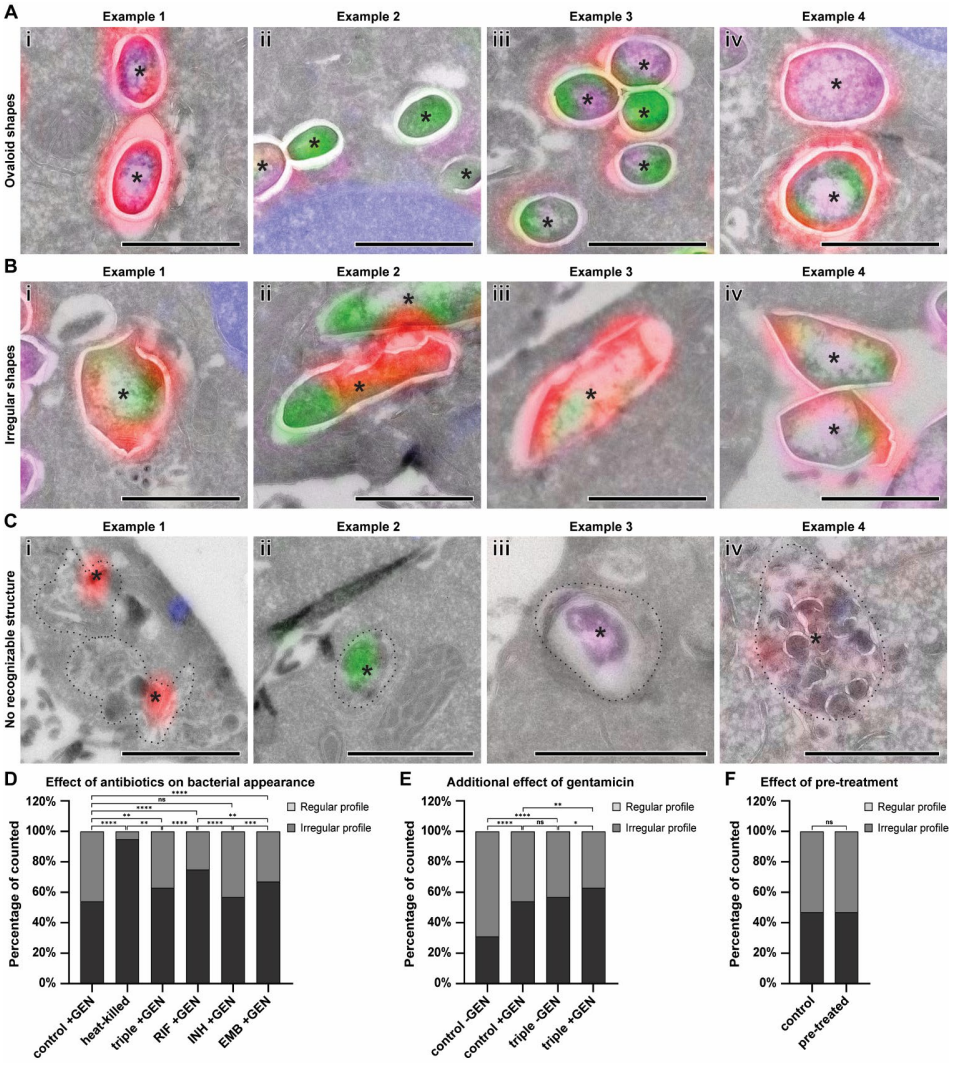

Figure S14. Intracellular *Mtb* displays bacterial profiles in various shapes. RAW 264.7 macrophages were infected with triple label *Mtb* for 1 hour (0h untreated) and incubated for 24 hours without antibiotics (24h control) or with rifampicin, isoniazid and ethambutol (24h triple antibiotics) and compared to *Mtb* pre-treated with triple antibiotics before infection (0h pre-treated). The variety of shapes, observed for the bacterial profiles, were classified into ovaloid (**A**) or irregular (**B**). In some cases, clear fluorescence was observed without any recognizable bacterial structure (**C**), containing either alkDala (**i**), Aha (**ii**), DsRed (**iii**) or all three combined (**iv**). Relevant structures are indicated with an asterisk (*). A dotted line indicates the apparent vacuole where relevant. All scale bars represent 1 µm. **D:** The intracellular appearance of *Mtb* was manually classified as ovaloid or irregular, shown as percentage relative to the total number of *Mtb* counted in the analyzed region; n>500 bacteria counted. **E:** The additional effect of gentamicin (GEN) on the intracellular appearance of *Mtb* was assessed after 24 hours of incubation with triple antibiotic cocktail (triple +/-GEN) or without antibiotics (control +/-GEN); n>500 bacteria counted. **F:** The early intracellular appearance of *Mtb* was assessed directly after infection with *Mtb* pre-treated with triple antibiotics cocktail or with untreated

control bacteria; n>200 bacteria counted. Raw distributions were pairwise compared using the chi-square test and corrected for multiple testing using the Benjamini-Hochberg procedure, with a false discovery rate (FDR) of 0.1 (****: p<0.0001, ***: p<0.001, **: p<0.01, *: p<0.05, ns: not significant).

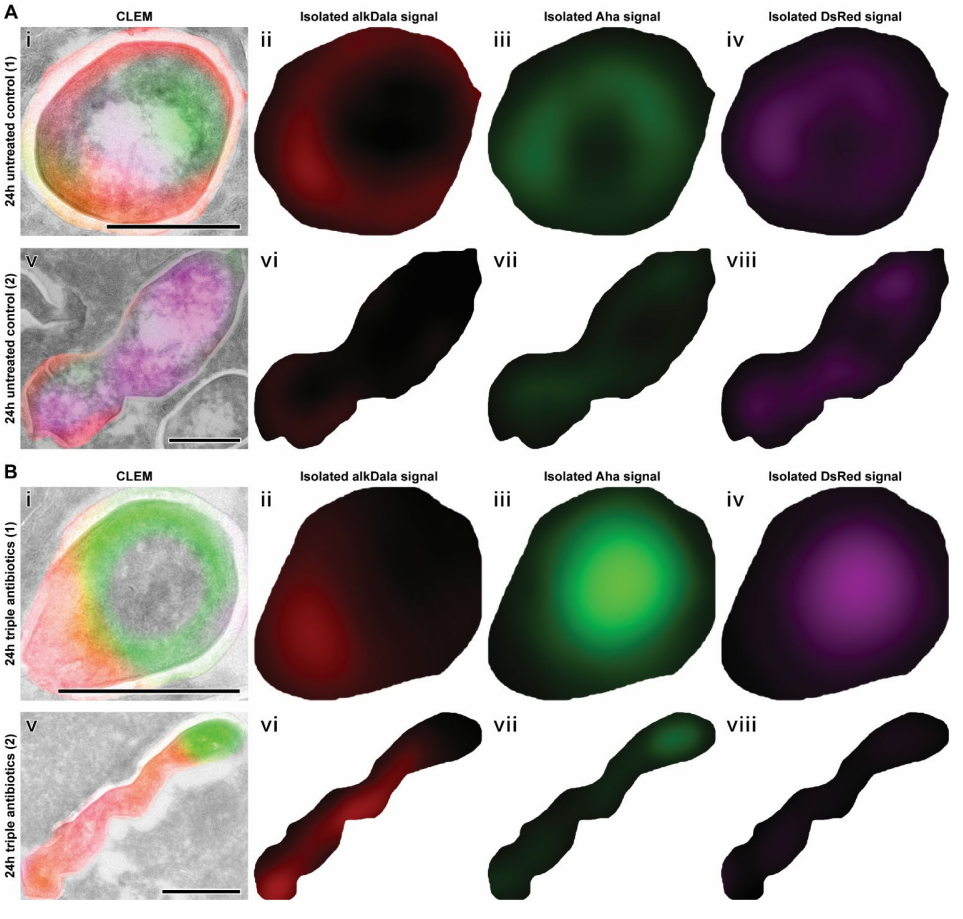

Figure S15. Semi-automatic CLEM-based quantification of label retention in intracellular *Mtb*. RAW 264.7 macrophages were infected with triple label *Mtb* for 1 hour and incubated for 24 hours with rifampicin, isoniazid and ethambutol (24h triple antibiotics) or no antibiotics (24h untreated control). The resulting confocal fluorescence image was correlated onto the corresponding large field of view (stitched) TEM image, using Photoshop. Bacterial outline was drawn manually in Photoshop, using the 'lasso tool', followed by automatic cropping and separation of channels, using a JavaScript. Raw fluorescence images (brightness/contrast unchanged) were subsequently analyzed based on the average fluorescence intensity of the non-white area (masked), using an ImageJ macro. **A:** Two examples of untreated control bacteria, incubated for 24 hours intracellularly without antibiotics, showing the color-merged CLEM image (**i,v**), isolated alkDala signal (**ii,vi**), isolated Aha signal (**iii,vii**) and isolated DsRed signal (**iv,viii**). **B:** Two examples of triple antibiotics treated bacteria, incubated for 24 hours intracellularly with rifampicin, isoniazid and ethambutol, showing the color-merged CLEM image (**i,v**), isolated alkDala signal (**ii,vi**), isolated Aha signal (**iii,vii**) and isolated DsRed signal (**iv,viii**). All scale bars represent 500 nm.

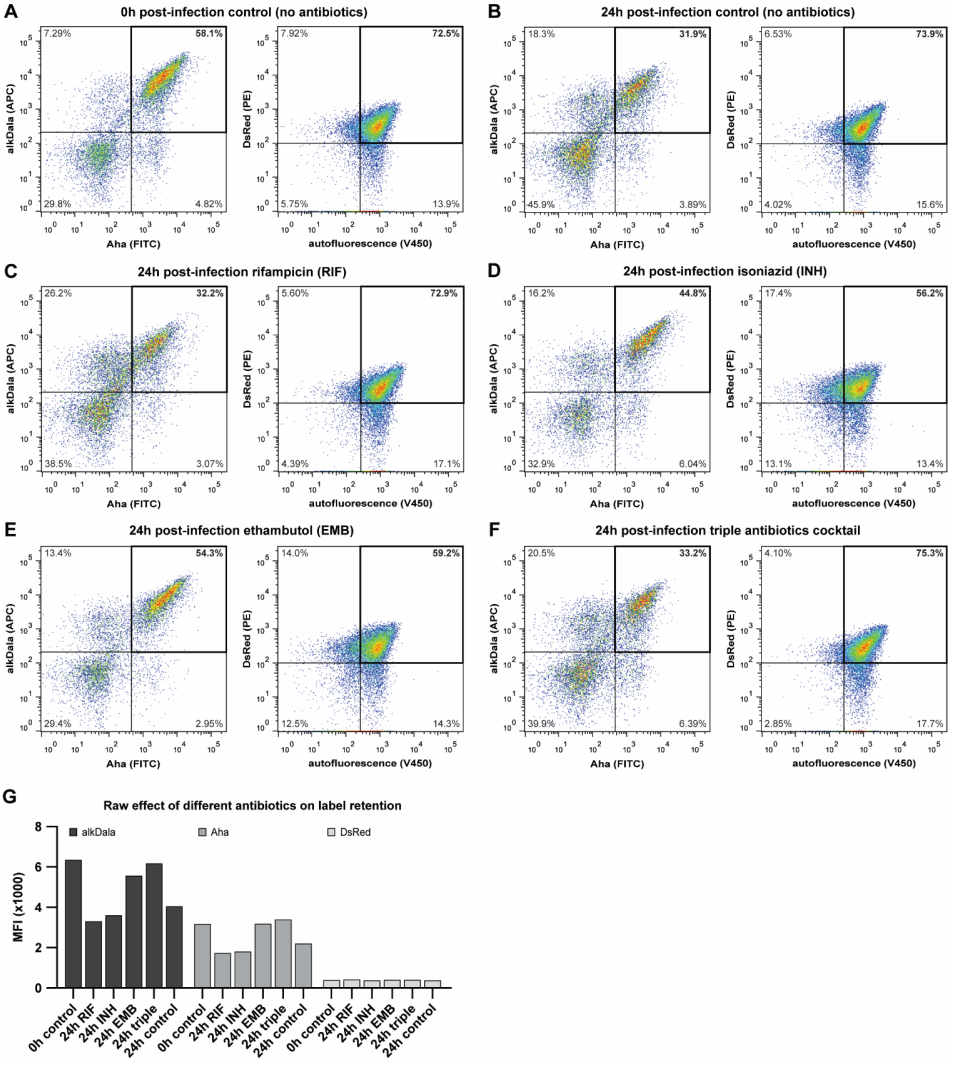

Figure S16. Quantification of label retention by flow cytometry. RAW 264.7 macrophages were infected with triple label *Mtb* for 1 hour (0h control; **A**) and further incubated for 24 hours without antibiotics (24h control; **B**) or with rifampicin (RIF; **C**), isoniazid (INH; **D**), ethambutol (EMB; **E**) or a combination of the three (triple; **F**). Bacteria were recovered by selective lysis of the host cell, fixed and processed for flow cytometry. The average label retention was quantified by selecting the Aha+/alkDala+ quadrant or the autofluorescence+/DsRed+ quadrant. **G:** The median fluorescence intensity (MFI) was used for the quantification of all signals, as it reflects the average signal intensity for a local population most accurately. Corresponding normalized MFI values are presented in Fig. 6B.

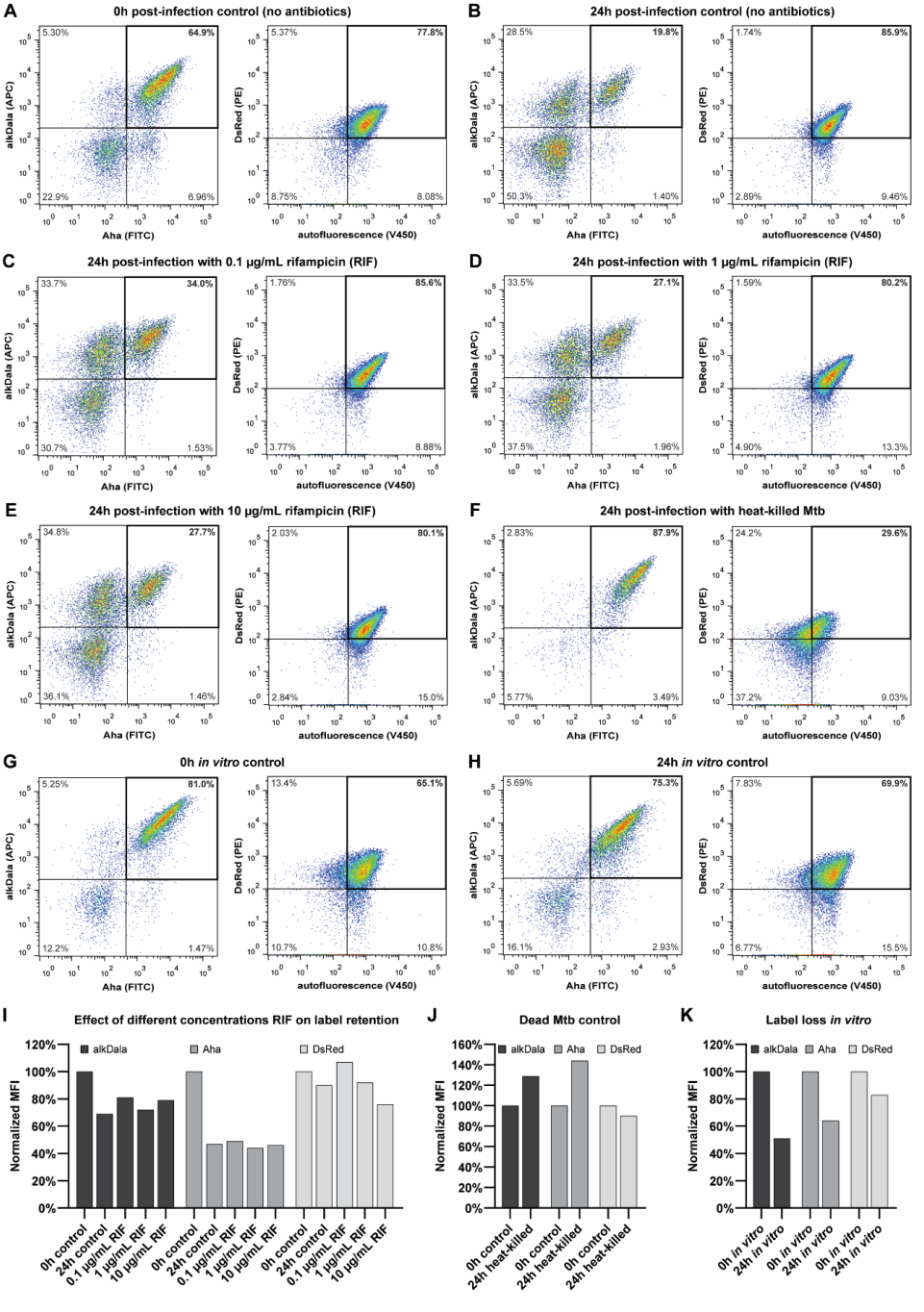

Figure S17. Additional controls for bacterial recovery from host cells. RAW 264.7 macrophages were infected with triple label *Mtb* for 1 hour (0h control; **A**) and further incubated for 24 hours without antibiotics (24h control; **B**) or with increasing concentrations of rifampicin (RIF; **C, D, E**) or heat-killed (30 min at 80°C) *Mtb*

(**F**). Bacteria were recovered by selective lysis of the host cell, fixed and processed for flow cytometry. Additional in vitro controls were included, in which the *Mtb* were incubated in cell medium for 0h (**G**) or 24h (**H**). The average label retention was quantified by selecting the Aha+/alkDala+ quadrant or the autofluorescence+/DsRed+ quadrant. **I/J/K:** MFI was used for the quantification of all signals and subsequently normalized to the 0h time point.

5.6 References

(1) World Health Organization. *Global Tuberculosis Report 2018*; **2018**.
(2) Fletcher, H. A.; Voss, G.; Casimiro, D.; Neyrolles, O.; Williams, A.; Kaufmann, S. H. E.; McShane, H.; Hatherill, M. Progress and Challenges in TB Vaccine Development. *F1000Research* **2018**, *7* (Mvi), 1–14.
(3) Schluger, N. W. Host-Pathogen Interactions in Tuberculosis: The Evolving Story. *J. Infect. Dis.* **2016**, *214* (8), 1137–1138.
(4) Bald, D.; Villellas, C.; Lu, P.; Koul, A. Targeting Energy Metabolism in Mycobacterium Tuberculosis, a New Paradigm in Antimycobacterial Drug Discovery. *MBio* **2017**, *8* (2), 1–11.
(5) Jnawali, H. N.; Ryoo, S. First – and Second – Line Drugs and Drug Resistance. In *Tuberculosis - Current Issues in Diagnosis and Management*; Mahboub, B. H., Vats, M. G., Eds.; InTech, **2013**; pp 163–180.
(6) Deb, C.; Lee, C.-M. M.; Dubey, V. S.; Daniel, J.; Abomoelak, B.; Sirakova, T. D.; Pawar, S.; Rogers, L.; Kolattukudy, P. E. A Novel in Vitro Multiple-Stress Dormancy Model for Mycobacterium Tuberculosis Generates a Lipid-Loaded, Drug-Tolerant, Dormant Pathogen. *PLoS One* **2009**, *4* (6), e6077.
(7) Dutta, N. K.; Karakousis, P. C. Latent Tuberculosis Infection: Myths, Models, and Molecular Mechanisms. *Microbiol. Mol. Biol. Rev.* **2014**, *78* (3), 343–371.
(8) Baker, J. J.; Abramovitch, R. B. Genetic and Metabolic Regulation of Mycobacterium Tuberculosis Acid Growth Arrest. *Sci. Rep.* **2018**, *8* (1), 4168.
(9) Daniel, J.; Maamar, H.; Deb, C.; Sirakova, T. D.; Kolattukudy, P. E. Mycobacterium Tuberculosis Uses Host Triacylglycerol to Accumulate Lipid Droplets and Acquires a Dormancy-like Phenotype in Lipid-Loaded Macrophages. *PLoS Pathog.* **2011**, *7* (6), e1002093.
(10) Pullan, S. T.; Allnutt, J. C.; Devine, R.; Hatch, K. A.; Jeeves, R. E.; Hendon-Dunn, C. L.; Marsh, P. D.; Bacon, J. The Effect of Growth Rate on Pyrazinamide Activity in Mycobacterium Tuberculosis - Insights for Early Bactericidal Activity? *BMC Infect. Dis.* **2016**, *16* (205), 1–11.
(11) Evangelopoulos, D.; Fonseca, J. D. da; Waddell, S. J. Understanding Anti-Tuberculosis Drug Efficacy: Rethinking Bacterial Populations and How We Model Them. *Int. J. Infect. Dis.* **2015**, *32*, 76–80.
(12) Sarathy, J. P.; Via, L. E.; Weiner, D.; Blanc, L.; Boshoff, H.; Eugenin, E. A.; Barry, C. E.; Dartois, V. A. Extreme Drug Tolerance of Mycobacterium Tuberculosis in Caseum. *Antimicrob. Agents Chemother.* **2018**, *62* (2), 1–11.
(13) Hoagland, D. T.; Liu, J.; Lee, R. B.; Lee, R. E. New Agents for the Treatment of Drug-Resistant Mycobacterium Tuberculosis. *Adv. Drug Deliv. Rev.* **2016**, *102*, 55–72.
(14) Sarkar, S.; Ganguly, A. Current Overview of Anti-Tuberculosis Drugs: Metabolism and Toxicities. *Mycobact. Dis.* **2016**, *6* (2), 1–6.
(15) Philips, J. a.; Ernst, J. D. Tuberculosis Pathogenesis and Immunity. *Annu. Rev. Pathol. Mech. Dis.* **2012**, *7* (1), 353–384.
(16) North, R. J.; Jung, Y.-J. Immunity to Tuberculosis. *Annu. Rev. Immunol.* **2004**, *22* (1), 599–623.
(17) Wilburn, K. M.; Fieweger, R. A.; VanderVen, B. C. Cholesterol and Fatty Acids Grease the Wheels of Mycobacterium Tuberculosis Pathogenesis. *Pathog. Dis.* **2018**, *76* (2), 1–14.
(18) Omotade, T. O.; Roy, C. R. Manipulation of Host Cell Organelles by Intracellular Pathogens. *Microbiol. Spectr.* **2019**, *7* (2), 1–18.
(19) van der Wel, N.; Hava, D.; Houben, D.; Fluitsma, D.; van Zon, M.; Pierson, J.; Brenner, M.; Peters, P. J. M. Tuberculosis and M. Leprae Translocate from the Phagolysosome to

the Cytosol in Myeloid Cells. *Cell* **2007**, *129* (7), 1287–1298.
(20) Zhai, W.; Wu, F.; Zhang, Y.; Fu, Y.; Liu, Z. The Immune Escape Mechanisms of Mycobacterium Tuberculosis. *Int. J. Mol. Sci.* **2019**, *20* (2).
(21) Ehrt, S.; Schnappinger, D. Mycobacterial Survival Strategies in the Phagosome: Defense against Host Stresses. *Cell Microbiol.* **2009**, *11* (8), 1170–1178.
(22) Schnettger, L.; Rodgers, A.; Repnik, U.; Lai, R. P.; Pei, G.; Verdoes, M.; Wilkinson, R. J.; Young, D. B.; Gutierrez, M. G. A Rab20-Dependent Membrane Trafficking Pathway Controls M. Tuberculosis Replication by Regulating Phagosome Spaciousness and Integrity. *Cell Host Microbe* **2017**, *21* (5), 619-628.e5.
(23) Simeone, R.; Bobard, A.; Lippmann, J.; Bitter, W.; Majlessi, L.; Brosch, R.; Enninga, J. Phagosomal Rupture by Mycobacterium Tuberculosis Results in Toxicity and Host Cell Death. *PLoS Pathog.* **2012**, *8* (2).
(24) Romagnoli, A.; Etna, M. P.; Giacomini, E.; Pardini, M.; Remoli, M. E.; Corazzari, M.; Falasca, L.; Goletti, D.; Gafa, V.; Simeone, R.; Delogu, G.; Piacentini, M.; Brosch, R.; Fimia, G. M.; Coccia, E. M. ESX-1 Dependent Impairment of Autophagic Flux by Mycobacterium Tuberculosis in Human Dendritic Cells. *Autophagy* **2012**, *8* (9), 1357–1370.
(25) Lerner, T. R.; Carvalho-Wodarz, C. D. S.; Repnik, U.; Russell, M. R. G.; Borel, S.; DIedrich, C. R.; Rohde, M.; Wainwright, H.; Collinson, L. M.; Wilkinson, R. J.; Griffiths, G.; Gutierrez, M. G. Lymphatic Endothelial Cells Are a Replicative Niche for Mycobacterium Tuberculosis. *J. Clin. Invest.* **2016**, *126* (3), 1093–1108.
(26) Kimmey, J. M.; Stallings, C. L. Bacterial Pathogens versus Autophagy: Implications for Therapeutic Interventions. *Trends Mol. Med.* **2016**, *22* (12), 1060–1076.
(27) MacGilvary, N. J.; Tan, S. Fluorescent Mycobacterium Tuberculosis Reporters: Illuminating Host-Pathogen Interactions. *Pathog. Dis.* **2018**, *76* (3), 1–12.
(28) Siegrist, M. S.; Whiteside, S.; Jewett, J. C.; Aditham, A.; Cava, F.; Bertozzi, C. R. D-Amino Acid Chemical Reporters Reveal Peptidoglycan Dynamics of an Intracellular Pathogen. *ACS Chem. Biol.* **2013**, *8* (3), 500–505.
(29) Botella, H.; Yang, G.; Ouerfelli, O.; Ehrt, S.; Nathan, C. F.; Vaubourgeix, J. Distinct Spatiotemporal Dynamics of Peptidoglycan Synthesis between Mycobacterium Smegmatis and Mycobacterium Tuberculosis. *MBio* **2017**, *8* (5), 12–14.
(30) Backus, K. M.; Boshoff, H. I.; Barry, C. E. C. S.; Boutureira, O.; Patel, M. K.; D'Hooge, F.; Lee, S. S.; Via, L. E.; Tahlan, K.; Barry, C. E. C. S.; Davis, B. G. Uptake of Unnatural Trehalose Analogs as a Reporter for Mycobacterium Tuberculosis. *Nat. Chem. Biol.* **2011**, *7* (4), 228–235.
(31) Hodges, H. L.; Brown, R. A.; Crooks, J. A.; Weibel, D. B.; Kiessling, L. L. Imaging Mycobacterial Growth and Division with a Fluorogenic Probe. *Proc. Natl. Acad. Sci. U. S. A.* **2018**, *115* (20), 5271–5276.
(32) Kamariza, M.; Shieh, P.; Ealand, C. S.; Peters, J. S.; Chu, B.; Rodriguez-Rivera, F. P.; Babu Sait, M. R.; Treuren, W. V.; Martinson, N.; Kalscheuer, R.; Kana, B. D.; Bertozzi, C. R. Rapid Detection of Mycobacterium Tuberculosis in Sputum with a Solvatochromic Trehalose Probe. *Sci. Transl. Med.* **2018**, *10* (430), eaam6310.
(33) Yang, D.; Ding, F.; Mitachi, K.; Kurosu, M.; Lee, R. E.; Kong, Y. A Fluorescent Probe for Detecting Mycobacterium Tuberculosis and Identifying Genes Critical for Cell Entry. *Front. Microbiol.* **2016**, *7* (DEC), 1–13.
(34) Cheng, Y.; Xie, H.; Sule, P.; Hassounah, H.; Graviss, E. A.; Kong, Y.; Cirillo, J. D.; Rao, J. Fluorogenic Probes with Substitutions at the 2 and 7 Positions of Cephalosporin Are Highly BlaC-Specific for Rapid Mycobacterium Tuberculosis Detection. *Angew. Chemie - Int. Ed.* **2014**, *53* (35), 9360–9364.
(35) Stone, M. R. L.; Butler, M. S.; Phetsang, W.; Cooper, M. A.; Blaskovich, M. A. T. Fluorescent Antibiotics: New Research Tools to Fight Antibiotic Resistance. *Trends*

Biotechnol. **2018**, *36* (5), 523–536.

(36) Cheng, Y.; Xie, J.; Lee, K.-H.; Gaur, R. L.; Song, A.; Dai, T.; Ren, H.; Wu, J.; Sun, Z.; Banaei, N.; Akin, D.; Rao, J. Rapid and Specific Labeling of Single Live *Mycobacterium Tuberculosis* with a Dual-Targeting Fluorogenic Probe. *Sci. Transl. Med.* **2018**, *10* (454), eaar4470.

(37) Armstrong, J. A.; D'Arcy Hart, P. Response of Cultured Macrophages to Mycobacterium Tuberculosis, with Observations on Fusion of Lysosomes with Phagosomes. *J Exp Med* **1971**, *134* (3), 713–740.

(38) Leake, E. S.; Myrvik, Q. N.; Wright, M. J. Phagosomal Membranes of Mycobacterium Bovis BCG-Immune Alveolar Macrophages Are Resistant to Disruption by Mycobacterium Tuberculosis H37Rv. *Infect. Immun.* **1984**, *45* (2), 443–446.

(39) McDonough, K. A.; Kress, Y.; Bloom, B. R. The Interaction of Mycobacterium Tuberculosis with Macrophages: A Study of Phagolysosome Fusion. *Infect. Agents Dis.* **1993**, *2* (4), 232–235.

(40) de Boer, P.; Hoogenboom, J. P.; Giepmans, B. N. G. Correlated Light and Electron Microscopy: Ultrastructure Lights Up! *Nat. Methods* **2015**, *12* (6), 503–513.

(41) Lerner, T. R.; Borel, S.; Greenwood, D. J.; Repnik, U.; Russell, M. R. G.; Herbst, S.; Jones, M. L.; Collinson, L. M.; Griffiths, G.; Gutierrez, M. G. Mycobacterium Tuberculosis Replicates within Necrotic Human Macrophages. *J. Cell Biol.* **2017**, *216* (3), 583–594.

(42) Russell, M. R. G.; Lerner, T. R.; Burden, J. J.; Nkwe, D. O.; Pelchen-Matthews, A.; Domart, M. C.; Durgan, J.; Weston, A.; Jones, M. L.; Peddie, C. J.; Carzaniga, R.; Florey, O.; Marsh, M.; Gutierrez, M. G.; Collinson, L. M. 3D Correlative Light and Electron Microscopy of Cultured Cells Using Serial Blockface Scanning Electron Microscopy. *J. Cell Sci.* **2017**, *130* (1), 278–291.

(43) Greenwood, D. J.; Dos Santos, M. S.; Huang, S.; Russell, M. R. G.; Collinson, L. M.; MacRae, J. I.; West, A.; Jiang, H.; Gutierrez, M. G. Subcellular Antibiotic Visualization Reveals a Dynamic Drug Reservoir in Infected Macrophages. *Science* **2019**, *364* (6447), 1279–1282.

(44) van Elsland, D. M.; Bos, E.; de Boer, W.; Overkleeft, H. S.; Koster, A. J.; van Kasteren, S. I. Detection of Bioorthogonal Groups by Correlative Light and Electron Microscopy Allows Imaging of Degraded Bacteria in Phagocytes. *Chem. Sci.* **2016**, *7* (1), 752–758.

(45) van Elsland, D. M.; Pujals, S.; Bakkum, T.; Bos, E.; Oikonomeas-Koppasis, N.; Berlin, I.; Neefjes, J.; Meijer, A. H.; Koster, A. J.; Albertazzi, L.; van Kasteren, S. I. Ultrastructural Imaging of Salmonella–Host Interactions Using Super-Resolution Correlative Light-Electron Microscopy of Bioorthogonal Pathogens. *ChemBioChem* **2018**, *19* (16), 1766–1770.

(46) Van Hest, J. C. M.; Kiick, K. L.; Tirrell, D. A. Efficient Incorporation of Unsaturated Methionine Analogues into Proteins in Vivo. *J. Am. Chem. Soc.* **2000**, *122* (7), 1282–1288.

(47) Kiick, K. L.; Saxon, E.; Tirrell, D. a; Bertozzi, C. R. Incorporation of Azides into Recombinant Proteins for Chemoselective Modification by the Staudinger Ligation. *Proc. Natl. Acad. Sci. U. S. A.* **2002**, *99* (1), 19–24.

(48) Dieterich, D. C.; Link, A. J.; Graumann, J.; Tirrell, D. A.; Schuman, E. M. Selective Identification of Newly Synthesized Proteins in Mammalian Cells Using Bioorthogonal Noncanonical Amino Acid Tagging (BONCAT). *Proc. Natl. Acad. Sci.* **2006**, *103* (25), 9482–9487.

(49) Hatzenpichler, R.; Scheller, S.; Tavormina, P. L.; Babin, B. M.; Tirrell, D. A.; Orphan, V. J. In Situ Visualization of Newly Synthesized Proteins in Environmental Microbes Using Amino Acid Tagging and Click Chemistry. *Environ. Microbiol.* **2014**, *16* (8), 2568–2590.

(50) Korbee, C. J.; Heemskerk, M. T.; Kocev, D.; Van Strijen, E.; Rabiee, O.; Franken, K. L. M. C.; Wilson, L.; Savage, N. D. L.; Džeroski, S.; Haks, M. C.; Ottenhoff, T. H. M. Combined

Chemical Genetics and Data-Driven Bioinformatics Approach Identifies Receptor Tyrosine Kinase Inhibitors as Host-Directed Antimicrobials. *Nat. Commun.* **2018**, *9* (1).

(51) Vincent, A. T.; Nyongesa, S.; Morneau, I.; Reed, M. B.; Tocheva, E. I.; Veyrier, F. J. The Mycobacterial Cell Envelope: A Relict from the Past or the Result of Recent Evolution? *Front. Microbiol.* **2018**, *9* (OCT), 1–9.

(52) Daffé, M.; Quémard, A.; Marrakchi, H. Mycolic Acids: From Chemistry to Biology. In *Biogenesis of Fatty Acids, Lipids and Membranes*; 2017; pp 1–36.

(53) Gengenbacher, M.; Kaufmann, S. H. E. Mycobacterium Tuberculosis: Success through Dormancy. *FEMS Microbiol. Rev.* **2012**, *36* (3), 514–532.

(54) Tokuyasu, K. T. A Technique for Ultracryotomy of Cell Suspensions and Tissues. *J. Cell Biol.* **1973**, *57* (2), 551–565.

(55) Peters, P. J.; Bos, E.; Griekspoor, A. Cryo-Immunogold Electron Microscopy. *Curr. Protoc. Cell Biol.* **2006**, *30* (1), 4.7.1-4.7.19.

(56) Möbius, W.; Posthuma, G. Sugar and Ice: Immunoelectron Microscopy Using Cryosections According to the Tokuyasu Method. *Tissue Cell* **2018**, No. July, 1–13.

(57) Gupta, A.; Bhakta, S. An Integrated Surrogate Model for Screening of Drugs against Mycobacterium Tuberculosis. *J. Antimicrob. Chemother.* **2012**, *67* (6), 1380–1391.

(58) Wang, X.; Grace, P. M.; Pham, M. N.; Cheng, K.; Strand, K. A.; Smith, C.; Li, J.; Watkins, L. R.; Yin, H. Rifampin Inhibits Toll-like Receptor 4 Signaling by Targeting Myeloid Differentiation Protein 2 and Attenuates Neuropathic Pain. *FASEB J.* **2013**, *27* (7), 2713–2722.

(59) Faas, F. G. A.; Cristina Avramut, M.; van den Berg, B. M.; Mieke Mommaas, A.; Koster, A. J.; Ravelli, R. B. G. Virtual Nanoscopy: Generation of Ultra-Large High Resolution Electron Microscopy Maps. *J. Cell Biol.* **2012**, *198* (3), 457–469.

(60) Vijay, S.; Hai, H. T.; Thu, D. D. A.; Johnson, E.; Pielach, A.; Phu, N. H.; Thwaites, G. E.; Thuong, N. T. T. Ultrastructural Analysis of Cell Envelope and Accumulation of Lipid Inclusions in Clinical Mycobacterium Tuberculosis Isolates from Sputum, Oxidative Stress, and Iron Deficiency. *Front. Microbiol.* **2018**, *8* (JAN), 1–12.

(61) Acosta, Y.; Zhang, Q.; Rahaman, A.; Ouellet, H.; Xiao, C.; Sun, J.; Li, C. Imaging Cytosolic Translocation of Mycobacteria with Two-Photon Fluorescence Resonance Energy Transfer Microscopy. *Biomed. Opt. Express* **2014**, *5* (11), 3990.

(62) Houben, D.; Demangel, C.; van Ingen, J.; Perez, J.; Baldeón, L.; Abdallah, A. M.; Caleechurn, L.; Bottai, D.; van Zon, M.; de Punder, K.; van der Laan, T.; Kant, A.; Bossers-de Vries, R.; Willemsen, P.; Bitter, W.; van Soolingen, D.; Brosch, R.; van der Wel, N.; Peters, P. J. ESX-1-Mediated Translocation to the Cytosol Controls Virulence of Mycobacteria. *Cell. Microbiol.* **2012**, *14* (8), 1287–1298.

(63) Simeone, R.; Sayes, F.; Song, O.; Gröschel, M. I.; Brodin, P.; Brosch, R.; Majlessi, L. Cytosolic Access of Mycobacterium Tuberculosis: Critical Impact of Phagosomal Acidification Control and Demonstration of Occurrence In Vivo. *PLoS Pathog.* **2015**, *11* (2), 1–24.

(64) Jamwal, S. V.; Mehrotra, P.; Singh, A.; Siddiqui, Z.; Basu, A.; Rao, K. V. S. Mycobacterial Escape from Macrophage Phagosomes to the Cytoplasm Represents an Alternate Adaptation Mechanism. *Sci. Rep.* **2016**, *6* (February), 1–9.

(65) Chandra, P.; Ghanwat, S.; Matta, S. K.; Yadav, S. S.; Mehta, M.; Siddiqui, Z.; Singh, A.; Kumar, D. Mycobacterium Tuberculosis Inhibits RAB7 Recruitment to Selectively Modulate Autophagy Flux in Macrophages. *Sci. Rep.* **2015**, *5* (October), 1–10.

(66) Abdallah, A. M.; Bestebroer, J.; Savage, N. D. L.; de Punder, K.; van Zon, M.; Wilson, L.; Korbee, C. J.; van der Sar, A. M.; Ottenhoff, T. H. M.; van der Wel, N. N.; Bitter, W.; Peters, P. J. Mycobacterial Secretion Systems ESX-1 and ESX-5 Play Distinct Roles in Host Cell Death and Inflammasome Activation. *J. Immunol.* **2011**, *187* (9), 4744–4753.

(67) Martin, C. J.; Booty, M. G.; Rosebrock, T. R.; Nunes-Alves, C.; Desjardins, D. M.; Keren,

I.; Fortune, S. M.; Remold, H. G.; Behar, S. M. Efferocytosis Is an Innate Antibacterial Mechanism. *Cell Host Microbe* **2012**, *12* (3), 289–300.

(68) Liu, Y.; Zhang, Q.; Hu, M.; Yu, K.; Fu, J.; Zhou, F.; Liu, X. Proteomic Analyses of Intracellular Salmonella Enterica Serovar Typhimurium Reveal Extensive Bacterial Adaptations to Infected Host Epithelial Cells. *Infect. Immun.* **2015**, *83* (7), 2897–2906.

(69) Patiño, S.; Alamo, L.; Cimino, M.; Casart, Y.; Bartoli, F.; García, M. J.; Salazar, L. Autofluorescence of Mycobacteria as a Tool for Detection of Mycobacterium Tuberculosis. *J. Clin. Microbiol.* **2008**, *46* (10), 3296–3302.

(70) Wong, C.; Ha, N. P.; Pawlowski, M. E.; Graviss, E. A.; Tkaczyk, T. S. Differentiating between Live and Dead Mycobacterium Smegmatis Using Autofluorescence. *Tuberculosis* **2016**, *101*, S119–S123.

(71) Shetty, A.; Dick, T. Mycobacterial Cell Wall Synthesis Inhibitors Cause Lethal ATP Burst. *Front. Microbiol.* **2018**, *9* (AUG), 1–9.

(72) Zhang, M. M.; Tsou, L. K.; Charron, G.; Raghavan, A. S.; Hang, H. C. Tandem Fluorescence Imaging of Dynamic S-Acylation and Protein Turnover. *Proc. Natl. Acad. Sci. U. S. A.* **2010**, *107* (19), 8627–8632.

(73) Li, N.; Lim, R. K. V; Edwardraja, S.; Lin, Q. Copper-Free Sonogashira Cross-Coupling for Functionalization of Alkyne-Encoded Proteins in Aqueous Medium and in Bacterial Cells. *J. Am. Chem. Soc.* **2011**, *133* (39), 15316–15319.

(74) Chenault, H. K.; Dahmer, J.; Whitesides, G. M. Kinetic Resolution of Unnatural and Rarely Occurring Amino Acids: Enantioselective Hydrolysis of N-Acyl Amino Acids Catalyzed by Acylase I. *J. Am. Chem. Soc.* **1989**, *111* (16), 6354–6364.

(75) Biagini, S. C. G.; Gibson, S. E.; Keen, S. P. Cross-Metathesis of Unsaturated Alpha-Amino Acid Derivatives. *J. Chem. Soc. Perkin Trans. 1* **1998**, *1*, 2485–2500.

(76) Dong, S.; Merkel, L.; Moroder, L.; Budisa, N. Convenient Syntheses of Homopropargylglycine. *J. Pept. Sci.* **2008**, *14* (10), 1148–1150.

(77) Schindelin, J.; Arganda-Carreras, I.; Frise, E.; Kaynig, V.; Longair, M.; Pietzsch, T.; Preibisch, S.; Rueden, C.; Saalfeld, S.; Schmid, B.; Tinevez, J. Y.; White, D. J.; Hartenstein, V.; Eliceiri, K.; Tomancak, P.; Cardona, A. Fiji: An Open-Source Platform for Biological-Image Analysis. *Nat. Methods* **2012**, *9* (7), 676–682.

(78) Wehrli, W. Rifampin: Mechanisms of Action and Resistance. *Rev. Infect. Dis.* **1983**, *5*, S407–S411.

(79) Timmins, G. S.; Deretic, V. Mechanisms of Action of Isoniazid. *Mol. Microbiol.* **2006**, *62* (5), 1220–1227.

(80) Goude, R.; Amin, A. G.; Chatterjee, D.; Parish, T. The Arabinosyltransferase EmbC Is Inhibited by Ethambutol in Mycobacterium Tuberculosis. *Antimicrob. Agents Chemother.* **2009**, *53* (10), 4138–4146.

(81) Yamori, S.; Ichiyama, S.; Shimokata, K.; Tsukamura, M. Bacteriostatic and Bactericidal Activity of Antituberculosis Drugs against Mycobacterium Tuberculosis, Mycobacterium Avium-Mycobacterium Intracellulare Complex and Mycobacterium Kansasii in Different Growth Phases. *Microbiol. Immunol.* **1992**, *36* (4), 361–368.

(82) Bakker-Woudenberg, I. A. J. M.; Van Vianen, W.; Van Soolingen, D.; Verbrugh, H. A.; Van Agtmael, M. A. Antimycobacterial Agents Differ with Respect to Their Bacteriostatic versus Bactericidal Activities in Relation to Time of Exposure, Mycobacterial Growth Phase, and Their Use in Combination. *Antimicrob. Agents Chemother.* **2005**, *49* (6), 2387–2398.

(83) Prokhorova, I.; Altman, R. B.; Djumagulov, M.; Shrestha, J. P.; Urzhumtsev, A.; Ferguson, A.; Chang, C. W. T.; Yusupov, M.; Blanchard, S. C.; Yusupova, G.; Puglisi, J. D. Aminoglycoside Interactions and Impacts on the Eukaryotic Ribosome. *Proc. Natl. Acad. Sci. U. S. A.* **2017**, *114* (51), E10899–E10908.

(84) McCollister, B. D.; Hoffman, M.; Husain, M.; Vázquez-Torres, A. Nitric Oxide Protects

Bacteria from Aminoglycosides by Blocking the Energy-Dependent Phases of Drug Uptake. *Antimicrob. Agents Chemother.* **2011**, *55* (5), 2189–2196.

(85) Batson, S.; De Chiara, C.; Majce, V.; Lloyd, A. J.; Gobec, S.; Rea, D.; Fülöp, V.; Thoroughgood, C. W.; Simmons, K. J.; Dowson, C. G.; Fishwick, C. W. G.; De Carvalho, L. P. S.; Roper, D. I. Inhibition of D-Ala:D-Ala Ligase through a Phosphorylated Form of the Antibiotic D-Cycloserine. *Nat. Commun.* **2017**, *8* (1), 1–7.

(86) Durrant, A. R.; Heresco-Levy, U. D-Cycloserine. In *Encyclopedia of Psychopharmacology*; Springer Berlin Heidelberg: Berlin, Heidelberg, **2013**; pp 1–5.